J. Fluid Mech. (1996), *vol.* 311, *pp.* 289–326

A computational analysis of electrohydrodynamics of a leaky dielectric drop in an electric field

By JAMES Q. FENG† AND TIMOTHY C. SCOTT

Chemical Technology Division, Oak Ridge National Laboratory, Oak Ridge, TN 37831-6224, USA

(Received 7 March 1995 and in revised form 31 October 1995)

Axisymmetric steady flows driven by an electric field about a deformable fluid drop suspended in an immiscible fluid are studied within the framework of the leaky dielectric model. Deformations of the drop and the flow fields are determined by solving the nonlinear free-boundary problem composed of the Navier–Stokes system governing the flow field and Laplace's system governing the electric field. The solutions are obtained by using the Galerkin finite-element method with an elliptic mesh generation scheme. Under conditions of creeping flow and vanishingly small drop deformations, the results of finite-element computations recover the asymptotic results. When drop deformations become noticeable, the asymptotic results are often found to underestimate both the flow intensity and drop deformation. By tracking solution branches in parameter space with an arc-length continuation method, curves in parameter space of the drop deformation parameter D versus the square of the dimensionless field strength E usually exhibit a turning point when E reaches a critical value E_c. Along such a family of drop shapes, steady solutions do not exist for $E > E_c$. The *nonlinear* relationship revealed computationally between D and E^2 appears to be capable of providing insight into discrepancies reported in the literature between experiments and predictions based on the asymptotic theory. In some special cases with fluid conductivities closely matched, however, drop deformations are found to grow with E^2 indefinitely and no critical value E_c is encountered by the corresponding solution branches. For most cases with realistic values of physical properties, the overall electrohydrodynamic behaviour is relatively insensitive to effects of finite-Reynolds-number flow. However, under extreme conditions when fluids of very low viscosities are involved, computational results illustrate a remarkable shape turnaround phenomenon: a drop with oblate deformation at low field strength can evolve into a prolate-like drop shape as the field strength is increased.

1. Introduction

When a fluid drop is suspended in another immiscible fluid, it can be influenced by an externally applied uniform electric field in many ways. If the fluids are considered as perfectly insulating dielectrics and no free charges are present at the fluid interface, or if, on the other hand, the drop contains a fluid that is highly conducting while the surrounding fluid is insulating, an electric field induces a net force at the fluid

† Also affiliated with the Department of Chemical Engineering, University of Tennessee. Present Address: Xerox Corporation, Wilson Center for Research & Technology, 800 Phillips Road, Webster, NY 14580, USA.

interface as a result of discontinuity in the electric field (cf. Melcher & Taylor 1969; Melcher 1981). Such an electric surface force always acts perpendicularly to the drop interface and points from the fluid of higher dielectric constant, or the conducting fluid, toward the fluid of lower dielectric constant, or the insulating fluid. Because this electric surface force acts only in the direction normal to the interface, it can be mechanically balanced by a uniform interfacial tension. Therefore, the fluids can remain motionless with the drop surface always being statically elongated in the direction of the electric field into a prolate shape. These ideal situations of electrified drops have been extensively studied within the well-established theoretical framework of *electrohydrostatics* (cf. O'Konski & Thacher 1953; Garton & Krasucki 1964; Taylor 1964; Rosenkilde 1969; Miksis 1981; Adornato & Brown 1983; Basaran & Scriven 1989). However, neither perfectly insulating fluids nor perfectly conducting fluids (except the superconductors formed at very low temperature) are found in the real world. Most applications deal with fluids of finite electrical conductivity.

The problem becomes more interesting yet complicated when finite conductivity of fluids is considered. Perhaps one of the most remarkable phenomena is the finding that, in addition to the prolate shape predicted by the electrohydrostatic theory, a drop in an electric field may be maintained in a spherical shape or even be deformed into an oblate spheroid as observed in many experiments (Buchner & Van Royen 1929; Bungenberg de Jong & Hoskam 1941; Allen & Mason 1962). Extending the electrohydrostatic theory to include the effects of finite conductivity of fluids, O'Konski & Harris (1957) suggested a mathematical expression, which, although incorrect, indicates the existence of conditions under which the drop might remain spherical or become an oblate spheroid. Taylor (1966) recognized that finite conductivity enables electrical charge to accumulate at the drop interface, permitting a tangential electric stress to be generated. The tangential electric stress drags fluids into motion, generating hydrodynamic stresses at the drop interface. The intricate interplay between the electric and hydrodynamic stresses can produce either oblate or prolate drop deformations, and can also maintain a spherical drop. The *electrohydrodynamic* theory proposed by Taylor (1966) is based on what came to be known as the leaky dielectric model, which is capable of predicting drop deformations in qualitative agreement with previous experimental observations.

However, extensive experiments conducted later by Torza, Cox & Mason (1971) showed serious quantitative discrepancy with Taylor's theoretical prediction. Drops were found to be consistently more deformed than would be expected from the theoretical prediction, in many cases by as much as a factor of two to four. To resolve the quantitative discrepancy between theory and experiment, the linearized asymptotic model of Taylor (1966) was extended to include higher-order terms by Ajayi (1978). Although Ajayi's more accurate theory indicates an increase in drop deformations, the higher-order correction was found to be insufficient to fully remove the discrepancy. To examine the issue of electrokinetic effects raised by Torza *et al.* (1971), the leaky dielectric model was replaced by an electrokinetic model of charge transport (Baygents & Saville 1989). Even though the microscale motions and diffused charge layers are more accurately described, the calculated drop deformation turns out to be exactly the same as that given by the leaky dielectric model. Thus, the leaky dielectric model is verified to be the correct lumped-parameter model when no net charge exists on the drop. Since none of the obvious theoretical extensions seemed to be able to resolve the serious discrepancy, Vizika & Saville (1992) carried out a further experimental investigation. Their results appeared to agree with the asymptotic leaky dielectric prediction better than previous experiments, although

certain discrepancies remain for some cases. Still, no consistent explanations have been provided for the lack of quantitative agreement between the leaky dielectric theory and experiment.

The experiments on the electrohydrodynamic behaviour of drops have been restricted to a small range of fluid properties because of the requirement of matching fluid densities necessary to avoid significant drop migrations driven by buoyancy. Accurate measurement and control of the electrical conductivity of weakly conductive fluids are difficult. On the other hand, for the sake of tractablility with conventional mathematical tools, the analytical solutions to date have been restricted to creeping flows around drops with small deformations in an infinitely extended domain. State-of-the-art computational techniques, however, have not yet been utilized to systematically gain further insights into the apparent discrepancy between the leaky dielectric theory and experiment. The greatest advantages of computational analyses lie in the fact that most of the restrictions introduced in the previous theoretical analyses to avoid severe nonlinearities can be removed, and physical parameters can easily be varied in an independent fashion, which is often difficult or impossible in a laboratory experiment. To make use of such advantages, this work is devoted to using the Galerkin finite-element method (cf. Strang & Fix 1973) to conduct a computational analysis of electrohydrodynamic behaviour of drops using the leaky dielectric model. By virtue of the generality of the numerical scheme, finite-Reynolds-number flows and large deformations of the drop interface can be examined systematically. The geometry of the problem domain can also be easily arranged to better approximate the realistic experimental situation.

Apart from basic scientific interest, knowledge of the electrohydrodynamics of drops has been playing an increasingly important role in practical applications. For example, some of the early studies were motivated by the importance of electrohydrodynamic deformation of drops in birefringence, light scattering, and other optical measurements of emulsion systems (cf. O'Konski & Thacher 1953; O'Konski & Harris 1957). More recent practical interest is associated with the processes in which enhancement of the rate of mass or heat transfer between drops and their surrounding fluid is desired (cf. Thornton 1968; Harker & Ahmadzadeh 1974; Bailes 1981; Baird 1983; Scott 1989; Weatherley 1992; Ptasinski & Kerkhof 1992; He, Baird & Chang 1993). Taking in account circulatory flows generated by an applied electric field, Morrison (1977) and Griffiths & Morrison (1979) evaluated transfer rate enhancement and found significant electroconvective effects for stationary drops. The numerical investigation of the electrohydrodynamic effects in transfer rate enhancement for spherical drops has been extended further to include both buoyancy-driven flows (Chang, Carleson & Berg 1982; Chang & Berg 1983) and interfacial tension gradients (Chang & Berg 1985). In the present work, we focus on the pure electrohydrodynamic effects on deformable drops under neutrally buoyant conditions, leaving other complications for future research.

It should be noted that some numerical computations have been performed on deformable leaky dielectric drops. For example, in investigating breakup modes of electrified drops, Sherwood (1988) considered finite conductivity effects and performed boundary-integral computations for prolate drops with the creeping-flow approximation. Besides dynamic details of the drop breakup process, Sherwood also presented steady prolate deformations of leaky dielectric drops for one case where highly deformed drops can maintain stable shapes under large electric field strength. In a study of electrohydrodynamic circulations inside and outside a neutrally suspended deformable drop, Tsukada *et al.* (1993) conducted computations with a finite-element

scheme that is somewhat similar to the one described in this work. Based on limited results, these authors claimed that their finite-element computations were in good agreement with Taylor's analytical results and their own experiments. Later, Tsukada *et al.* (1994) also reported some results for a leaky dielectric system with a drop moving in a quiescent liquid at small Reynolds number. However, none of these papers (i.e. Sherwood 1988; Tsukada *et al.* 1993, 1994) clearly addressed the issue of the quantitative discrepancy between Taylor's asymptotic theory and experiment.

One of the goals of this work is to establish a general relationship between drop deformations and applied electric field strength, based on numerical solutions of the mathematical system of the leaky dielectric model with minimal simplifying assumptions. Furthermore, this work also attempts to provide new insights into the complicated nonlinear behaviour of deformable drops with electrohydrodynamic flows, by exploring new phenomena that have not yet been observed in experiments. In §2 we present the nonlinear mathematical system of equations and boundary conditions that govern the steady electrohydrodynamic flow about a leaky dielectric drop driven by an externally applied electric field. The Galerkin finite-element methodology for discretizing and solving the free-boundary problem is described in §3. The solutions at the limit of creeping flow are analysed in §4, where the accuracy of computational results is verified by comparison with the asymptotic theory of Taylor (1966) for small drop deformations. The stability of drop shapes with respect to axisymmetric disturbances is inferred by considering the connectivity of the shape families (Iooss & Joseph 1990; Ungar & Brown 1982), which are efficiently tracked in parameter space with arc-length continuation methods (e.g. Keller 1977; Abbott 1978). With the numerical scheme of the Galerkin finite-element method, electrohydrodynamic flows at finite Reynolds number are investigated in §5, where dramatic changes in the electrohydrodynamic drop behaviour are explored. In §6, electric field distributions around drops and their relationship to the electrohydrodynamic flow intensity are discussed. A comparison of the computational results with the experimental data is presented in §7. With realistic values of fluid properties, the computational curves in parameter space show deviation from the asymptotic lines to capture the general trend of the experimental data. Finally in §8, we conclude with a discussion of the new findings obtained by the present computational analysis and offer suggestions for future research.

2. Mathematical formulation

We consider an axisymmetric fluid drop of volume $\frac{4}{3}\pi a^3$, viscosity μ_i, electrical conductivity σ_i, and dielectric constant κ_i, suspended in an immiscible fluid of viscosity μ_o, electrical conductivity σ_o, and dielectric constant κ_o. The drop is situated in the middle of a parallel-plate capacitor and is subjected to an electric field in the axial direction generated by imposing a voltage difference between the capacitor plates, which are separated by a distance L (figure 1). The densities of the two fluids are identical, denoted by ρ, so that the drop is under neutrally buoyant conditions even in an Earth-bound laboratory. The interface separating the two fluids has constant interfacial tension γ. Variables are made dimensionless by measuring lengths in units of the radius of the undeformed spherical drop a, electrical potential V in units of $(\gamma a/\epsilon_0)^{1/2}$, with ϵ_0 denoting the permittivity of vacuum, and velocity $\boldsymbol{u}$ in units of a characteristic velocity U defined later by (2.15) as the maximum surface velocity calculated from the creeping-flow solution for a spherical drop (Taylor 1966). In what follows, the subscript o denotes variables associated with the fluid outside the

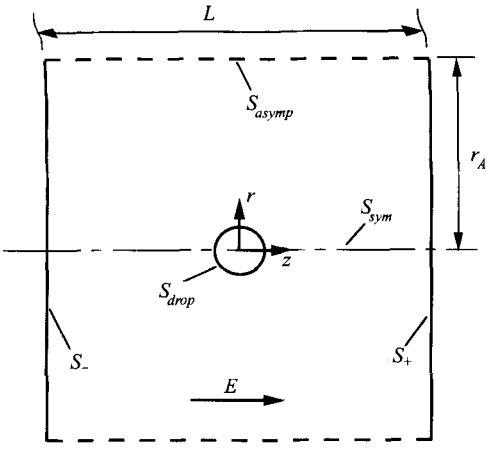

FIGURE 1. Schematic of the problem description: a drop neutrally buoyant in an immiscible fluid is subjected to a uniform electric field at the middle of a parallel-plate capacitor.

drop and the subscript i denotes those associated with the fluid inside the drop. The variables without subscript o or i apply in either phase.

The electric field $\boldsymbol{E} \equiv -\nabla V$ is determined by solving the steady-state equation of charge conservation,

$$\nabla \cdot \boldsymbol{J} = 0, \tag{2.1}$$

where $\boldsymbol{J} = -(\sigma/\sigma_o)\nabla V$ is the dimensionless electrical current density due to ohmic conduction. In this work, the convection of charge by fluid flow is assumed to be negligible, following Taylor's treatment (1966), which is generally valid for the situation of very small electric Reynolds number, i.e., $\epsilon_0 \kappa U/(\sigma a) \ll 1$ (cf. Melcher & Taylor 1969; Melcher 1981). Because the conductivities σ_i and σ_o are constants, equation (2.1) becomes Laplace's equation for V in each fluid region.

At the drop interface, the requirements of continuity of the tangential component of the electric field and that of the normal component of the electrical current density, as consistent with charge conservation when charge convection by flow is neglected, are described by the boundary conditions

$$V_i = V_o \quad \text{and} \quad \frac{\sigma_i}{\sigma_o}\, \boldsymbol{n}\cdot\nabla V_i = \boldsymbol{n}\cdot\nabla V_o \quad \text{on} \quad S_{drop}, \tag{2.2}$$

where $\boldsymbol{n}$ is the local unit normal vector to the boundary. The continuity of the normal component of the current density does not prevent the surface charge from appearing at the drop interface; instead, it ensures that the amount of local surface charge does not vary with time. In the present formulation, surface charge does not appear explicitly anywhere, because the equations are written in terms of the current density instead of electric displacement.

At the capacitor plates located at $z = L/2$ and $z = -L/2$, constant electric potentials are imposed in the form of Dirichlet boundary conditions as

$$V_o = -E\frac{L}{2} \quad \text{on} \quad S_+ \quad \text{and} \quad V_o = E\frac{L}{2} \quad \text{on} \quad S_-. \tag{2.3}$$

Moreover, a Neumann boundary condition for the electric field is applied along the axis of symmetry and the asymptotic boundary,

$$\boldsymbol{n}\cdot\nabla V = 0 \quad \text{on} \quad S_{sym} \quad \text{and} \quad S_{asymp}. \tag{2.4}$$

Unlike the usual boundary-value problems in electrostatic theory where the domain shapes are known *a priori*, the electric field around the deformable drop cannot be determined unless the shape of the drop interface is described. In the present free-boundary problem, the drop shape can be influenced by stresses arising from both the electric field and fluid flows. Hence, the equations describing fluid flows must be considered simultaneously.

The incompressible fluid motions in both phases are governed by the steady Navier–Stokes equations

$$Re\ \boldsymbol{u}\cdot\nabla\boldsymbol{u} = \nabla\cdot\boldsymbol{T}, \tag{2.5}$$

and continuity equation

$$\nabla\cdot\boldsymbol{u} = 0. \tag{2.6}$$

Here $Re \equiv \rho a U/\mu_o$ is the Reynolds number of the flow outside the drop, and the hydrodynamic stress tensor for the exterior phase takes the form

$$\boldsymbol{T}_o = -p_o\boldsymbol{I} + [\nabla\boldsymbol{u}_o + (\nabla\boldsymbol{u}_o)^T], \tag{2.7a}$$

whereas the hydrodynamic stress tensor for the interior phase is given by

$$\boldsymbol{T}_i = -p_i\boldsymbol{I} + \frac{\mu_i}{\mu_o}[\nabla\boldsymbol{u}_i + (\nabla\boldsymbol{u}_i)^T], \tag{2.7b}$$

where p_o and p_i are the pressures outside and inside the drop, and $\boldsymbol{I}$ is the identity tensor. The fluids here are assumed to be Newtonian with uniform viscosities. Both the stress and the pressure are measured in units of $\mu_o U/a$.

At the drop interface, conservation of momentum is expressed by the traction boundary condition

$$\boldsymbol{n}\cdot(\boldsymbol{T}_o - \boldsymbol{T}_i) = \frac{1}{Ca}\left[\left(\frac{\mathrm{d}\boldsymbol{t}}{\mathrm{d}s} + \frac{\boldsymbol{n}}{r}\frac{\mathrm{d}z}{\mathrm{d}s}\right) - \boldsymbol{n}\cdot(\boldsymbol{T}_o^e - \boldsymbol{T}_i^e)\right], \quad \text{on } S_{drop}, \tag{2.8}$$

where $Ca \equiv \mu_o U/\gamma$ is the capillary number, $\boldsymbol{t}$ is the local unit tangential vector to the boundary (in an azimuthal plane), and s is the arc-length along the boundary. Here $\boldsymbol{n}$ points into the drop and $\boldsymbol{t}$ points in the direction of increasing s that corresponds to increasing the polar angle measured from the negative z-axis; therefore, $\boldsymbol{n}\cdot\mathrm{d}\boldsymbol{t}/\mathrm{d}s + (1/r)(\mathrm{d}z/\mathrm{d}s)$ is the sum of the local principal mean curvatures. The Maxwell stress tensor

$$\boldsymbol{T}^e = \kappa(\boldsymbol{E}\,\boldsymbol{E} - \tfrac{1}{2}\boldsymbol{I}\,\boldsymbol{E}\cdot\boldsymbol{E}) \tag{2.9}$$

accounts not only for the electric stresses that are attributable to free charges, but also for those due to polarization (cf. Melcher & Taylor 1969; Melcher 1981).

The drop interface can be regarded as a material surface, provided there is no mass transfer across it. At steady state, the kinematic condition at the drop interface is then simply

$$\boldsymbol{n}\cdot\boldsymbol{u} = 0 \quad \text{on } S_{drop}. \tag{2.10}$$

Also, the continuity of velocity at the drop interface requires

$$\boldsymbol{u}_o = \boldsymbol{u}_i \quad \text{on } S_{drop}. \tag{2.11}$$

At the surface of capacitor plates, the fluid must obey no-slip and no-penetration conditions,

$$\boldsymbol{u} = 0 \quad \text{on } S_+ \text{ and } S_-. \tag{2.12}$$

Along the axis of symmetry, the symmetry conditions are exprected to be satisfied

$$\frac{dz}{ds} = 0 \quad \text{at} \quad r = 0 \quad \text{on} \quad S_{drop}, \quad \text{and} \quad \boldsymbol{e}_z \boldsymbol{e}_r : \boldsymbol{T} = \boldsymbol{e}_r \cdot \boldsymbol{u} = 0 \quad \text{on} \quad S_{sym}, \tag{2.13}$$

where $\boldsymbol{e}_z$ and $\boldsymbol{e}_r$ are unit vectors in the z- and r-directions, respectively.

Far from the drop, the electrohydrodynamic flows should vanish, i.e.

$$\boldsymbol{u} \to 0 \quad \text{and} \quad p \to 0 \quad \text{on} \quad S_{asymp} \quad \text{as} \quad r_A \to \infty. \tag{2.14}$$

The mathematical system defined by (2.1)–(2.14) involves the dimensionless parameters Re, Ca, $\mathscr{S} = \kappa_o/\kappa_i$, $\mathscr{M} = \mu_o/\mu_i$, and $\mathscr{R} = \sigma_i/\sigma_o$, where the notation for dielectric constant ratio $\mathscr{S}$, viscosity ratio $\mathscr{M}$, and conductivity ratio $\mathscr{R}$ is taken from Taylor's original work (1966). Based on Taylor's results for creeping flows around spherical drops, the maximum surface velocity, used here as the characteristic velocity in SI units (m s^{-1}) for our non-dimensionalization, can then be written as

$$U \equiv \frac{9|\mathscr{S}\mathscr{R} - 1|}{10(2 + \mathscr{R})^2(1 + \mathscr{M})} \frac{\kappa_i \gamma}{\mu_i} E^2, \tag{2.15}$$

where E, as in (2.3), is the dimensionless strength of electric field measured in units of $[\gamma/(\epsilon_0 a)]^{1/2}$.

3. Galerkin finite-element methodology

The nonlinear free-boundary problem composed of (2.1)–(2.14) is solved numerically by the Galerkin finite-element method. The solution is expedited by adopting special techniques developed for analysing viscous free-surface flows (cf. Kistler & Scriven 1983; Christodoulou & Scriven 1989, 1992; Christodoulou 1990; de Santos 1991), and those for studying electrohydrostatic and magnetohydrostatic problems (cf. Basaran 1984; Boudouvis 1987; Boudouvis, Puchalla, & Scriven 1988; Basaran & Scriven 1989). The numerical code used in this work is modified and enhanced with respect to that previously developed for analysing electrostatic effects in coating flows (Feng & Scriven 1992, 1993).

The axisymmetric problem domain depicted in figure 1 is subdivided into a set of quadrilateral elements (cf. Strang & Fix 1973), as shown in figure 2, with the elements adjacent to the centre of the drop having one side collapsed to a point at the origin in the physical space. On each element, which is mapped onto a unit square in the ξ,η domain, the unknown values of the electric potential and velocity fields are expressed in an expansion of biquadratic basis functions, whereas the pressure field is expressed in an expansion of linear discontinuous basis functions, i.e. the discretization of the flow field is accomplished in the mixed interpolation sense (Huyakorn *et al.* 1978) to avoid overconstraint problems due to the nature of the continuity equation (2.6). To facilitate the simultaneous solution of the electric potential and flow fields with free interface deformations, an elliptic mesh generation scheme (Thompson, Warsi & Mastin 1985) developed by Christodoulou & Scriven (1992) and modified by de Santos (1991) is employed. In essence, this method determines the locations of the nodal or mesh points of the finite-element grids by solving a pair of elliptic partial differential equations

$$\nabla \cdot D_\xi \nabla \xi = 0, \quad \nabla \cdot D_\eta \nabla \eta = 0, \tag{3.1}$$

where the 'mesh diffusion' coefficients D_ξ and D_η are adjustable functions of position that can be prescribed to meet a desired distribution of nodal or mesh points in the problem domain.

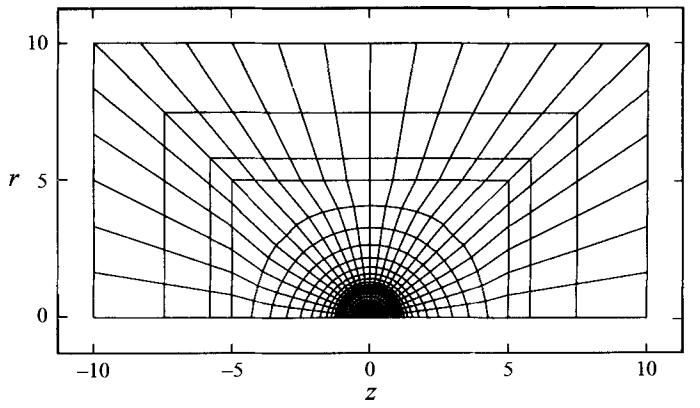

FIGURE 2. Typical finite element tesselation of the problem domain.

With the present computational scheme, S_{asymp} is positioned at a finite distance from the drop where the boundary conditions are not exactly known. However, it is often convenient to impose the boundary conditions

$$\boldsymbol{n}\,\boldsymbol{n} : \nabla \boldsymbol{u} = 0 \quad \boldsymbol{t}\,\boldsymbol{n} : \nabla \boldsymbol{u} = 0, \quad \text{and} \quad p = 0 \quad \text{on} \quad S_{asymp}, \tag{3.2}$$

which can be readily restated as a Neumann boundary conditions in terms of stresses. Although the boundary conditions (3.2) seem to be somewhat *ad hoc*, any errors incurred on S_{asymp} should be inconsequential to the essential electrohydrodynamic behaviour, provided that r_A is located reasonably far away from the drop where the flow velocity is vanishingly small. Neumann boundary conditions corresponding to (3.2) are preferred here over the Dirichlet conditions given by (2.14) because numerical errors incurred at S_{asymp} are easily relaxed.

To avoid variations in the drop volume that might arise from the inevitable presence of numerical errors, especially when the flow velocity vanishes at low electric field strength such that the kinematic condition (2.10) becomes trivial, we impose an equation of volume constraint

$$\int_{S_{drop}} r^2 \frac{\mathrm{d}z}{\mathrm{d}s}\,\mathrm{d}s = \frac{4}{3}. \tag{3.3}$$

This constraint requires an additional degree of freedom in the mathematical system, which is obtained by specifying a fixed value of pressure at one of the nodes inside the drop. This amounts to adding an undetermined pressure jump across the interface Δp_0 in the interfacial boundary condition (2.8), with pressure level being set for the fluid outside the drop through the boundary condition (3.2).

In a parallel-plate capacitor, the neutrally buoyant drop must be positioned exactly at the centre in order to maintain mechanical equilibrium. Unfortunately, such an equilibrium is unstable, i.e. the drop would drift toward one of the capacitor plates indefinitely should it deviate slightly from its equilibrium position. To prevent this kind of drift from destroying the steady-state solutions, we also require that the centre of mass of the drop remain at the coordinate origin

$$\int_{S_{drop}} r^2 z \frac{\mathrm{d}z}{\mathrm{d}s}\,\mathrm{d}s = 0. \tag{3.4}$$

With the constraint (3.4), another additional degree of freedom is required to complete

the mathematical description. The variable associated with this additional degree of freedom should represent some kind of force that prevents the drop from drifting and is vanishingly weak when the centre of mass of the drop approaches the coordinate origin. Our choice here is to define an artificial hydrostatic pressure that, in our dimensionless representation, appears to be an added term $\boldsymbol{n}zBo/Ca$ in the interfacial traction condition (2.8), where $Bo \equiv \Delta\rho g a^2/\gamma$ is the Bond number with g denoting the acceleration due to gravity. Thus, an artificial mismatch in fluid densities $\Delta\rho$ always compensates for whatever errors arising from the numerical processes that cause the drop's centre of mass to deviate from the coordinate origin. In fact, the magnitude of St determined by computations is always below our numerical error criterion for the convergence of solutions, e.g. 10^{-6}.

If one takes advantage of the mirror symmetry with respect to the equatorial plane, the size of the computational problem can be reduced by one-half. Then, the condition (3.4) becomes unnecessary because the drop now cannot freely translate along the symmetry axis with the imposed symmetry condition for the free interface at the point where it meets the equatorial plane and the constraint of constant drop volume (e.g. Tsukada *et al.* 1993). However, the mathematically imposed symmetry conditions at the equatorial plane make it impossible to detect the existence of drop shapes that are asymmetric with respect to the equatorial plane. Asymmetric shapes have indeed been found previously in oscillating drops in a system having similar symmetry. As shown theoretically by Feng (1991) and Feng & Beard (1991), a neutrally buoyant conducting drop subjected to an external force that is symmetric with respect to the equatorial plane, due to an alternating electric field, can oscillate with odd-number-lobed shapes when excited through the subharmonic resonance mechanism. It would be impossible to find those odd-number-lobed shapes of forced drop oscillations if the symmetry conditions were imposed at the equatorial plane. Therefore, we avoid imposition of those symmetry boundary conditions along the equatorial plane by keeping the general axisymmetric problem domain as shown in figure 2.

The Galerkin finite-element statement of the problem is completed by imposing boundary conditions on the mesh generation equations (3.1). Here, along the drop surface and the boundaries that are parallel to the drop surface in the computational domain, equal arc-length spacing of grid points is imposed with Dirichlet conditions on the relevant mesh generation equations. On the boundaries that are perpendicular to the drop surface in the computational domain, Dirichlet conditions are imposed with non-uniform D_ξ or D_η so that grid points are compressed toward the drop surface where viscous boundary layers are expected (e.g. de Santos 1991).

Once the mathematical system is completely described, Galerkin's method is applied by weighting the governing equations (2.1) and (2.5) with biquadratic basis functions used for the electric potential and velocity expansions, (2.6) with linear discontinuous basis functions used for the pressure expansion, and (3.1) with the appropriate finite-element basis functions for the subparametric mapping (Christodoulou & Scriven 1992). The equations weighted by the finite-element basis functions are then integrated over the entire physical domain, and the divergence theorem is utilized to lower the order of derivatives in the Laplace, momentum, and elliptic mesh generation equations. The Galerkin method of weighted residuals transforms the partial differential system into a set of nonlinear algebraic equations with finite degrees of freedom, which is then solved iteratively by Newton's method (cf. Ortega & Rheinboldt 1970). At each Newton's iteration, the resulting linear algebra system is solved by direct factorization of the Jacobian matrix with a modification of Hood's frontal solver (Hood 1976; Walters 1980).

Critical to Newton's method is the initial estimate of the solution, which must be accurate enough to fall within the domain of convergence of the method. A convenient start-up solution or initial estimate is obtained here by solving the governing equations under conditions of very small E, and therefore vanishingly small Re and Ca. Thus, interfacial tension is relatively large compared to other forces so that the profile of the drop interface is well approximated by an arc of a circle. Thereafter, steady-solution families are tracked efficiently by first-order continuation (Riks 1972; Keller 1977) in E. The Jacobian matrix becomes singular at turning points and, also, at certain bifurcation points in parameter space (cf. Iooss & Joseph 1990), and first-order continuation cannot lead to a converged solution. To continue along a solution branch past a turning point (which is the only kind of singular point encountered in this work), an arc-length continuation method (Keller 1977; Abbott 1978) is adopted. Thus, the critical values of E at turning points can be determined accurately.

The size of the gap between the capacitor plates and the location of the asymptotic boundary S_{ASYMP} are chosen to be $L = 20$ and $r_A = 10$, so that imposition of boundary conditions (2.3), (2.4), (2.12), and (3.2) at a finite distance from the drop induces virtually no difference between the computed solutions for $Re = 0$ and Taylor's asymptotic results when the drop takes the spherical shape as Taylor's discriminating function

$$\Phi \equiv \mathscr{S}(\mathscr{R}^2 + 1) - 2 + 3(\mathscr{S}\mathscr{R} - 1)\frac{2\mathscr{M} + 3}{5\mathscr{M} + 5} \tag{3.5}$$

approaches zero. The domain is divided into 600 elements with 2500 nodes. With the mesh used in this work, the total number of unknowns is 10 545. Typically, five steps of Newton iterations suffice to bring the L_2 norm of the error in the solution and residuals down to 10^{-6}. Increasing the size of the computational domain or number of elements deployed in the tessellation alters the location of the turning points in parameter space reported in the following sections by less than 1%.

In this work, most computations for the theoretical analysis are performed with parameter values based on interfacial tension $\gamma = 0.001\,\mathrm{N\,m^{-1}}$ and drop radius $a = 0.001\,\mathrm{m}$, corresponding roughly to the lowest interfacial tension and largest drops found in the experimental works of Torza *et al.* (1971) and Vizika & Saville (1992). Thus, the largest possible deformations representing realistic situations can be conveniently examined. For the sake of simplicity, most results are computed here with $\mathscr{M} = 1$, except when the effects of $\mathscr{M}$ are to be examined. The maximum strengths of the applied electric field used in the experiments (cf. Torza *et al.* 1971; Vizika & Saville 1992) were usually given in terms of aE^{*2} (here E^* denotes dimensional electric field strength) as on the order of $\sim 10^8\,\mathrm{V^2\,m^{-1}}$. This value becomes 0.941 in terms of our dimensionless field strength $E \equiv E^*(\epsilon_0 a/\gamma)^{1/2}$ (with $\epsilon_0 = 8.854 \times 10^{-12}\,\mathrm{F\,m^{-1}}$). Because typical values of γ in the experimental systems are often greater than 0.001 $\mathrm{N\,m^{-1}}$ (cf. Torza *et al.* 1971; Vizika & Saville 1992), $E = 1$ can be taken as the upper limit that is practically achievable under normal laboratory conditions. Hence, most of the results presented in this work are computed for $E \leqslant 1$. The values of dielectric constants are chosen to be either $\kappa_o = 5$ and $\kappa_i = 2.5$ or $\kappa_o = 2.5$ and $\kappa_i = 5$, which are representative of systems with liquids of low electrical conductivity, such as the castor oil and silicone oil used in the experiments (cf. Torza *et al.* 1971; Vizika & Saville 1992). Furthermore, our present attention focuses mainly on the systems with $\mathscr{R} \geqslant 10$ for $\mathscr{S} < 1$ and $\mathscr{R} \leqslant 0.1$ for $\mathscr{S} > 1$, consistent with most experiments conducted so far. A few cases with parameter values outside the above-mentioned ranges are, however, computed in the theoretical analysis and briefly discussed for illustrative

purposes. On the other hand, when comparisons are made with experimental data in §7, realistic values of fluid properties taken from the available experimental data are used in the computations.

4. Solutions at the limit of creeping flow

When inertia forces are not important and Re is set equal to zero, the Navier–Stokes equations reduce to the linear Stokes equation that describes axisymmetric creeping flows. By virtue of the simplicity of the Stokes equation, Taylor (1966) obtained analytical solutions for both the electric field and the creeping-flow field around spherical drops and then derived an asymptotic expression for the drop deformations. Maintaining the creeping-flow approximation, Ajayi (1978) extended Taylor's linear asymptotic theory to include higher-order effects on drop deformations. These analytical results provide valuable guidance for further computational analysis. First of all, estimates of the locations of S_{asymp}, S_+, and S_- can be obtained without tedious trial-and-error procedures, such that the numerical solutions yield essentially the same results as the analytical solutions for nearly spherical drops in an infinitely extended domain. Secondly, qualitative effects of physical factors are explicitly shown in the analytical formulas, so that the interpretation of complicated behaviour revealed by numerical solutions is made relatively easy.

From Taylor's asymptotic results we learn that, in the far field, the rate of decay for velocity is $\sim 1/r^2$, in a manner similar to the flow induced by a point-force dipole (e.g. Pozrikidis 1992). Thus, positioning the outer boundaries at dimensionless distance 10 from the drop invokes only 1% errors in the local velocity, which is already of very small magnitude. On the other hand, the analytical solution for a leaky dielectric sphere in a uniform electric field shows that the deviation of the electric potential from that of the uniform field vanishes at a rate of $1/r^3$ as $r \to \infty$. Therefore, the results computed with the present problem domain of finite size are also representive of the generic situation with the infinitely extended domain.

Setting Re to zero is implemented numerically by setting fluid density to zero. The computational results should therefore reasonably represent circumstances where the value of Re is very small. With $Re = 0$ and

$$Ca \equiv \mu_o U/\gamma = \frac{9|\mathscr{S}\mathscr{R} - 1|\mathscr{M}}{10(2+\mathscr{R})^2(1+\mathscr{M})}\kappa_i E^2, \tag{4.1}$$

the actual value of viscosity does not mathematically appear in the creeping-flow solutions. For most cases in this section where the viscosity ratio $\mathscr{M}$ is set equal to unity, the value of viscosity $\mu = \mu_o = \mu_i$ is set to 0.01 N s m^{-2} (ten times that of water).

4.1. *Creeping-flow fields with significant drop deformations*

Representative creeping-flow fields and drop shapes, shown in figure 3, are qualitatively consistent with the asymptotic theory of Taylor (1966). When $\mathscr{S}\mathscr{R} < 1$, the electric shear stress induces a pole-to-equator flow (see figure 3*a*, *b*, *d* and *f*), whereas the reversed flow pattern is induced when $\mathscr{S}\mathscr{R} > 1$ (see figure 3*c* and *e*). When $\mathscr{S}\mathscr{R} = 1$, the mathematical system (2.1)–(2.4) governing the electrical current density becomes exactly the same as the one governing the electric displacement field, $\kappa\nabla V$. Hence, requiring continuity of the normal component of the electrical current density given by (2.4) also enforces continuity of the normal component of the electric displacement field. Consequently, no net surface charge should appear in this particular

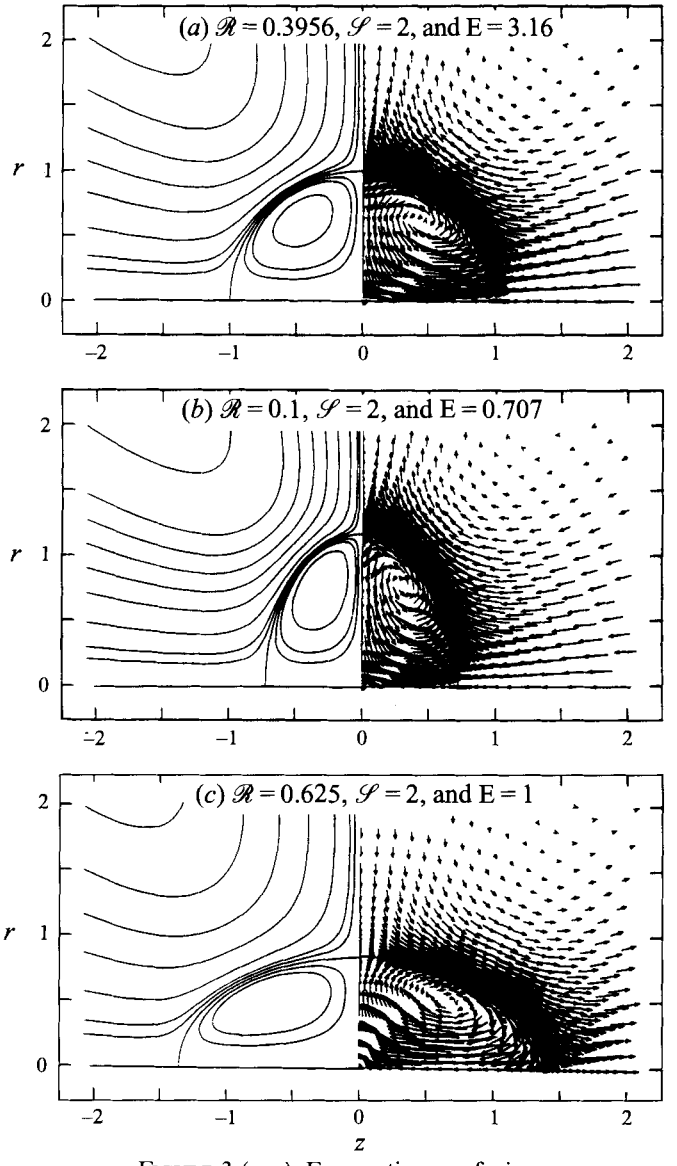

FIGURE 3 (*a–c*). For caption see facing page

circumstance, and electric shear stress at the drop interface vanishes as the value of $\mathscr{S}\mathscr{R}$ approaches unity (cf. Taylor 1966). Evaluated under the condition of $\mathscr{S}\mathscr{R} = 1$, Taylor's discriminating function (3.5), $\Phi = (\mathscr{R}+1)^2/\mathscr{R} > 0$, indicates that a prolate deformation always occurs in the absence of the flows induced by the electric shear stress. This makes $\mathscr{S}\mathscr{R} < 1$, corresponding to a pole-to-equator flow, a necessary condition for the drops to exhibit oblate deformations or remain the spherical shape, as seen from figure 3(*a, b, d, f*).

For most liquid–liquid systems, $\mathscr{R}$ can vary by many orders of magnitude, whereas the variation of $\mathscr{S}$ is in practice limited to $0.031 < \mathscr{S} < 32$ (according to $2.5 \leqslant \kappa \leqslant 80$). It is then roughly correct to expect prolate deformations when the drop is more

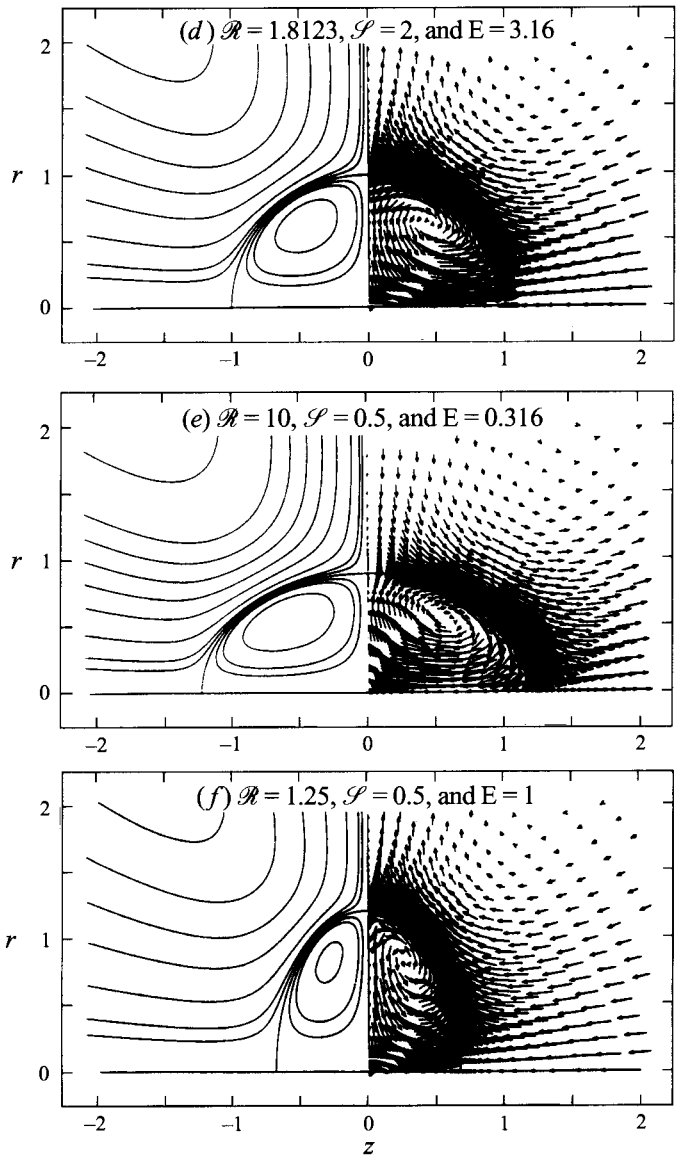

FIGURE 3. Electrohydrodynamic flows about a deformable drop at $Re = 0$ with $\mu_i = \mu_o = 0.01$ N s m^{-2}. By virtue of the problem symmetry, half of each plot shows the streamlines while the other half shows the velocity vectors. For illustrative purposes, the values of streamlines are chosen to be $\pm 0.01, \pm 0.02, \pm 0.05, \pm 0.1, \pm 0.15, \pm 0.2, \pm 0.25, \pm 0.3$, and ± 0.4. Depending upon the flow intensity in each individual case, not all the streamlines corresponding to the chosen values are necessarily shown in the plots.

conductive than the surrounding fluid, a phenomenon that becomes guaranteed when $\mathscr{R} > 10.2$ according to (3.5). For oblate deformations to occur, however, stringent conditions must be satisfied. Even with the most favourable values of $\mathscr{R}$ and $\mathscr{M}$ such as $\mathscr{R} \to 0$ and $\mathscr{M} \to 0$, Taylor's discriminating function still demands that at least $\mathscr{S} < 3.8$ be satisfied.

To quantitatively compare the computational results with the asymptotic predic-

tions, the computed maximum flow velocity and drop deformation parameter are examined. By virtue of our definition of the characteristic velocity (2.15), the maximum flow velocity $|\boldsymbol{u}|_{max}$ would remain at unit magnitude should the solutions quantitatively agree with that obtained by Taylor (1966). Following Taylor's definition, the deformation parameter is written as

$$D \equiv \frac{z_{max} - r_{max}}{z_{max} + r_{max}}, \tag{4.2}$$

where z_{max} is the maximum distance between the drop surface and the centre of mass of the drop along the direction of the applied electric field and r_{max} is that in the direction perpendicular to the applied electric field. Expressed in terms of Taylor's asymptotic results, an explicit relationship between D and E turns out to be

$$D = D_a = \frac{9\kappa_i \Phi}{16(2 + \mathscr{R})^2} E^2. \tag{4.3}$$

Listed in table 1 are the values of the computed maximum velocity $|\boldsymbol{u}|_{max}$ measured in units of U and the deformation parameter D with $Re = 0$ and $\mathscr{M} = 1$, for various combinations of $\mathscr{R}$ and $\mathscr{S}$ at several selected values of E. For convenience of comparison, the asymptotic prediction of the deformation parameter given by (4.3) is also included. Excellent agreement between our computational results and those obtained from Taylor's asymptotic theory (1966) is demonstrated by the fact that the computed maximum velocity is close to unity, as long as the drop deformation is insignificant, i.e. $D \sim 0$. When $\Phi \sim 0$, the computed drop profile maintains sphericity even at values of E^2 as large as 10 where $|D|$ is found to be only about 10^{-3}. Once there is a noticeable drop deformation, however, the computed maximum velocity deviates significantly from unity, and the deformation parameter D deviates from D_a. Hence, even at $Re = 0$, Taylor's asymptotic results for creeping flows around undeformed drops become inaccurate in describing the flow field when drop deformations are noticeable.

For a given field strength E, the drop deformation always appears to be more pronounced than that predicted by the asymptotic formula (4.3) when $|\boldsymbol{u}|_{max} > 1$ and less pronounced when $|\boldsymbol{u}|_{max} < 1$ (see table 1). This finding indicates that the drop deformation is directly related to the flow intensity for those cases. Deformations that are less pronounced than those predicted by Taylor's asymptotic theory have rarely been observed in experiments. Torza *et al.* (1971) reported only more pronounced deformations. It is noteworthy, however, that some corresponding cases of oblate drops reported by Torza *et al.* (1971) were shown by Vizika & Saville (1992) to exhibit somewhat less pronounced deformations. According to our computational results, less pronounced deformations are likely to occur when the conductivity ratio $\mathscr{R}$ approaches unity. No experiments to date have been conducted with systems of fluids of such closely matched conductivity. Difficulties are expected in experimenting with values of $\mathscr{R}$ close to unity because of the need to accurately measure and control the fluid conductivities.

4.2. *Critical strength of the electric field at turning points*

Figure 4 shows the evolution of the deformation parameter with E^2 for a few representative cases: $\mathscr{R} \geqslant 10$ with $\mathscr{S} = 0.5$, and $\mathscr{R} \leqslant 0.1$ with $\mathscr{S} = 2$. Typically along each solution branch there is a critical strength of the applied electric field E_c beyond which no steady solutions exist. However, more than one steady solution can exist at a value of $E < E_c$ – an example of multiple solutions for a given set of conditions in

E	$\mathscr{R}$	$\mathscr{S}$	Φ	$\|\boldsymbol{u}\|_{max}$	D	D_a
0.1	0.3956	2.0	-2.0×10^{-4}	0.9972	$\|D\| < 10^{-5}$	-4.93×10^{-7}
	0.10	2.0	-1.180	1.0023	-3.75×10^{-3}	-3.76×10^{-3}
	0.625	2.0	1.156	0.9983	2.38×10^{-3}	2.36×10^{-3}
	1.8123	0.5	1.4×10^{-3}	1.0005	$\|D\| < 10^{-5}$	2.79×10^{-6}
	10.0	0.5	54.50	1.0244	1.09×10^{-2}	1.06×10^{-2}
	1.25	0.5	-1.281	0.9981	-3.42×10^{-3}	-3.41×10^{-3}
0.316	0.3956	2.0	-2.0×10^{-4}	0.9972	$\|D\| < 10^{-5}$	-4.93×10^{-6}
	0.10	2.0	-1.180	1.0478	-3.78×10^{-2}	-3.76×10^{-2}
	0.625	2.0	1.156	0.9860	2.35×10^{-2}	2.36×10^{-2}
	1.8123	0.5	1.4×10^{-3}	1.0006	$\|D\| < 10^{-5}$	2.79×10^{-5}
	10.0	0.5	54.50	1.3922	0.1536	0.1063
	1.25	0.5	-1.281	0.9879	-3.32×10^{-2}	-3.41×10^{-2}
0.707	0.3956	2.0	-2.0×10^{-4}	0.9971	7.50×10^{-5}	-2.47×10^{-5}
	0.10	2.0	-1.180	1.2855	-0.2396	-0.1881
	0.625	2.0	1.156	0.9203	0.1163	0.1179
	1.8123	0.5	1.4×10^{-3}	1.0006	7.50×10^{-5}	1.40×10^{-4}
	10.0	0.5	54.50	–	–	0.5315
	1.25	0.5	-1.281	0.9112	-0.1534	-0.1705
1.0	0.3956	2.0	-2.0×10^{-4}	0.9971	1.50×10^{-4}	-4.93×10^{-5}
	0.10	2.0	-1.180	–	–	-0.3763
	0.625	2.0	1.156	0.8087	0.2297	0.2360
	1.8123	0.5	1.4×10^{-3}	1.0006	1.50×10^{-4}	2.79×10^{-4}
	10.0	0.5	54.50	–	–	1.063
	1.25	0.5	-1.281	0.7683	-0.2846	-0.3412

TABLE 1. Computed maximum velocity $|\boldsymbol{u}|_{max}$ and deformation parameter D

the present nonlinear system. At the critical field strength E_c, a mathematical singular point – the turning point – is approached, indicating the incipience of instability (cf. Iooss & Joseph 1990). Here the physical manifestation of the instability is that the stresses at the drop interface, arising from the electric field and the flow, become so strong that interfacial tension can no longer hold the interface together once the applied field strength is increased beyond E_c. Electrohydrodynamic burst was observed by Torza *et al.* (1971) with both prolate and oblate drops at large electric field strength. Computations of the detailed behaviour of electrohydrodynamic burst with prolate drops were performed by Sherwood (1988) for cases of $\mathscr{S} = 1$ and $\mathscr{R} = 20$ and 25, with the creeping-flow approximation and a boundary-integral technique. Electrohydrodynamic flows near the tips of highly elongated drops in a strong electric field were found to prevent the formation of conical tips, and the leaky dielectric drops tend to break into blobs.

The critical field strength E_c at turning points for leaky dielectric systems has not been previously determined by theoretical analyses or experimental measurements; typical values of E_c and corresponding deformation parameter D computed here for $Re = 0$ and $\mathscr{M} = 1$ with $\mu_i = \mu_o = 0.01\,\mathrm{N\,s\,m^{-2}}$ are, therefore, listed in table 2 for future reference. Increasing the contrast of conductivity between the two fluids leads to an increasing amount of electrical charge at the drop interface for the electric field to act upon and therefore tends to result in more pronounced drop deformations at a given electric field strength and to reduce the critical field strength for the incipience of drop instability. Particularly, when the drop is much more conductive than the

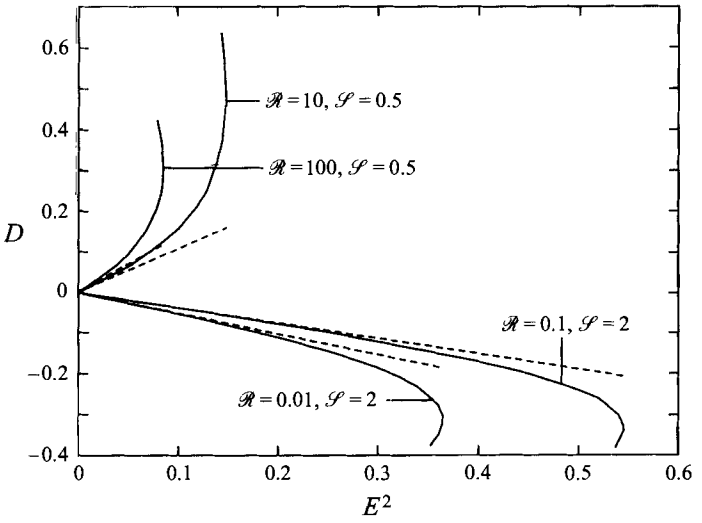

FIGURE 4. Steady-state solution branches of families in the parameter space of D as a function of E^2 for $\mathscr{R} = 0.01$ and 0.1 with $\mathscr{S} = 2$ and $\mathscr{R} = 10$ and 100 with $\mathscr{S} = 0.5$ at $Re = 0$ and $\mu_i = \mu_o = 0.01\ \mathrm{N\,s\,m^{-2}}$. Solid curves represent computational results, whereas dashed lines are the asymptotic results given by (4.3).

surrounding fluid for the case of $\mathscr{S} = 0.5$, the value of the critical field strength at the turning point approaches that for the electrohydrostatic situation of a perfectly conducting drop in a perfectly insulating fluid which is equal to 0.2879 (cf. Basaran & Scriven 1989; also Taylor 1964). Thus, for systems with large $\mathscr{R}$ (e.g. $\mathscr{R} \geqslant 100$), the effects of electrohydrodynamic flows become inconsequential and the system behaves just as if an uncharged conducting drop in an insulating fluid were subjected to an external electric field. A similar insensitivity of the system to the value of $\mathscr{R}$ for $\mathscr{R} \leqslant 0.01$ with $\mathscr{S} = 2.0$ is also found to be true for the inverse case where oblate drops are formed. For instance, the critical field strength is 0.6040 when $\mathscr{R} = 0.01$ and changes only slightly to 0.5931 when $\mathscr{R} = 0.001$.

To illustrate the general effects of viscosity ratio on the electrohydrodynamic behaviour, we evaluate the variation of the critical field strength E_c corresponding to the change in the value of $\mathscr{M}$. As shown in table 3, the values of critical field strength monotonically increase with the value of $\mathscr{M}$. Hence, the drops become more vulnerable to the externally applied electric field when the interior fluid is more viscous than the surrounding fluid. Taylor's asymptotic results indicate that relatively more significant effects of hydrodynamic stresses can be obtained by reducing the value of $\mathscr{M}$. Hence, a corollary may be derived that the hydrodynamic stresses due to fluid flows tend to enhance drop deformations, which is at least true in the common situations represented here, i.e. pole-to-equator flows with oblate drop deformations and equator-to-pole flows with prolate drop deformations. For the case of prolate drops with $\mathscr{S} = 0.5$ and $\mathscr{R} = 100$, not much change occurs in E_c when $\mathscr{M}$ varies from 0.1 to 10. This finding is in accord with the fact that, when the fluid inside the drop is much more conductive than that of the surrounding phase, the stresses resulting from the electrostatic field play the dominant role, while the hydrodynamic stresses due to fluid flows are relatively insignificant. Therefore, the general system behaviour can actually be well approximated and described by the much simpler treatment of electrohydrostatic theory. If the electrical properties of the system are inverted such

$\mathscr{R}$	$\mathscr{S}$	Φ	$\|\boldsymbol{u}\|_{max}$	E_c	D_c	D_a
0.10	2.0	−1.180	1.3569	0.7387	−0.3341	−0.2053
0.01	2.0	−1.470	1.4711	0.6040	−0.3130	−0.1866
0.001	2.0	−1.497	1.4785	0.5931	−0.3102	−0.1849
10.0	0.5	54.50	2.2899	0.3860	0.4719	0.1586
100.0	0.5	5072.0	2.5258	0.2939	0.3035	0.1185
1000.0	0.5	5.01×10^5	2.8357	0.2866	0.2956	0.1151

TABLE 2. Values of critical field strength E_c and corresponding deformation parameter D_c

μ_o (N s m^{-2})	μ_i (N s m^{-2})	$\mathscr{M}$	E_c	D_c
	$\mathscr{R} = 100$ and $\mathscr{S} = 0.5$			
0.01	0.1	0.1	0.2928	0.3043
0.01	0.01	1	0.2939	0.3035
0.1	0.01	10	0.2954	0.3100
	$\mathscr{R} = 0.01$ and $\mathscr{S} = 2$			
0.01	0.1	0.1	0.5575	−0.3026
0.01	0.01	1	0.6040	−0.3130
0.1	0.01	10	0.7029	−0.3777

TABLE 3. Variations of values of E_c and corresponding D_c with $\mathscr{M}$

that $\mathscr{S} = 2$ and $\mathscr{R} = 0.01$, the electrohydrodynamic behaviour becomes much more sensitive to the variation of the value of $\mathscr{M}$. Because the hydrodynamic stresses are essential to maintaining the oblate drop deformations against the prolate-inducing normal electric stress, the value of the viscosity ratio can significantly influence the electrohydrodynamic behaviour of oblate drops.

Clearly, the linear relationship between the deformation parameter D and E^2 with a constant slope $\mathrm{d}D/\mathrm{d}(E^2)$ as predicted by (4.3) is valid only asymptotically for small drop deformations; it cannot adequately describe the electrohydrodynamic behaviour when drop deformations are noticeable, especially when a turning point is approached. Near a turning point, both $|D|$ and $|\mathrm{d}D/\mathrm{d}(E^2)|$ rapidly increase with E^2, until the solution branch passes the turning point and folds back to lower values of E^2. Although seeking higher-order corrections through regular perturbation treatment (e.g. Ajayi 1978) points in the right direction, the inaccuracy of the perturbation formula with a limited number of expansion terms is expected to become much more serious in the vicinity of a turning point. Thus, fitting the experimental data with a straight line may be inherently inappropriate – a point that will be taken up further in §7.

4.3. *Special cases when asymptotic results may be valid at large E*

In those systems in which the fluid conductivities are closely matched, i.e. $\mathscr{R} = 0.625$ for $\mathscr{S} = 2.0$ and $\mathscr{R} = 1.25$ for $\mathscr{S} = 0.5$, the drops are less deformed than would be predicted by (4.3), and the corresponding solution branches extend beyond $E^2 = 1$, as can be seen in figure 5. If a solution branch is always confined by the corresponding line given by (4.3), it can never reach any turning points based on topological connectivity in two-dimensional parameter space. Our solutions computed beyond $E^2 = 1$ do not indicate that any critical points will appear. At least within $E \leqslant 1$, the

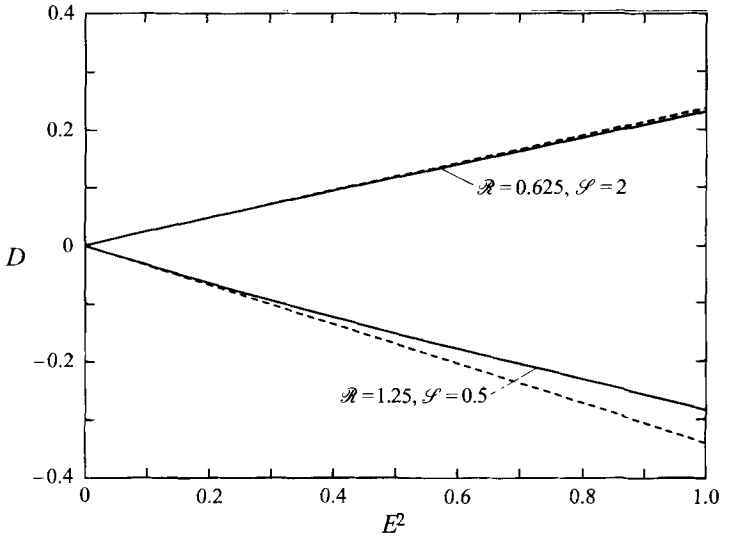

FIGURE 5. Steady-state solution branches of families in the parameter space of D as a function of E^2 for $\mathscr{R} = 0.625$ with $\mathscr{S} = 2$ and $\mathscr{R} = 1.25$ with $\mathscr{S} = 0.5$ at $Re = 0$ and $\mu_i = \mu_o = 0.01\,\mathrm{N\,s\,m^{-2}}$. Solid curves represent computational results, whereas dashed lines are the asymptotic results given by (4.3).

computed deformation parameter D varies almost linearly with E^2 and closely follows the corresponding asymptotic line, especially in the case with $\mathscr{R} = 0.625$ and $\mathscr{S} = 2.0$, where the computational results and the asymptotic ones are almost identical. Thus, the behaviour of these special systems may be well described by the asymptotic results even at large strengths of the applied electric field. For the cases computed here, the drop deformations tend to grow indefinitely as field strength increases. Similar behaviour was shown by Sherwood (1988) for the case of $\mathscr{S} = 1$ and $\mathscr{R} = 5$, where the drop deformation was found to increase smoothly with the applied field strength without causing the drop to burst. The indefinite growth of drop deformations with applied field strength was also found in the perfectly insulating fluid systems when the contrast of dielectric constants becomes less pronounced (cf. Rosenkilde 1969; Miksis 1981). However, the behaviour of leaky dielectric systems seems to be primarily determined by the ratio of conductivities, $\mathscr{R}$, whereas in the perfectly insulating systems the behaviour is governed by the ratio of dielectric constants, $\mathscr{S}$.

5. Solutions at finite Re

The Reynolds number Re becomes non-zero when a finite value is given for fluid density. The characteristic density used here is chosen to be $\rho = 10^3\,\mathrm{kg\,m^{-3}}$, because most liquids have densities of the same order as that of water. Both $Re \equiv \rho a U/\mu_o$ and $Ca \equiv \mu_o U/\gamma$ vary with E according to the change of U with E through (2.15). Explicitly, we can write

$$Re \equiv \frac{9|\mathscr{S}\mathscr{R} - 1|\rho a}{10(2+\mathscr{R})^2(1+\mathscr{M})}\frac{\kappa_i \gamma}{\mu_o \mu_i}E^2. \tag{5.1}$$

Unlike the solutions for creeping flow, in which Re is set to zero by assuming that $\rho = 0$ where the actual value of viscosity has no role to play, the value of μ in (5.1)

can significantly influence the value of Re for specified values of ρ and a. Therefore, we examine the inertial effects by conveniently varying the value of μ alone with the creeping-flow restriction removed.

5.1. *Cases when* $Re \leqslant O(1)$

If $\mu = \mu_o = \mu_i = 0.01\,\mathrm{N\,s\,m^{-2}}$, $\mathscr{S} = 0.5$ (i.e. $\kappa_o = 2.5$ and $\kappa_i = 5$), and $\mathscr{R} = 100$, we have

$$U = 1.06 \times 10^{-3} E^2 (\mathrm{m\,s^{-1}}) \quad \text{and} \quad Re = 0.106 E^2 \tag{5.2}$$

for $a = 0.001$ m and $\gamma = 0.001\,\mathrm{N\,m^{-1}}$. Because the critical field strength E_c is found to be 0.2939 for $Re = 0$, the Reynolds number in this case remains small for all achievable electric field strengths. As expected, the results computed with $Re \neq 0$ are the same as those computed at the limit of creeping flow. If $\mathscr{R}$ is reduced from 100 to 10 with everything else unchanged, $Re = 0.625E^2$. Although increased somewhat from that given by (5.2), the value of Re in this case still remains small because $E_c = 0.3860$ as given in table 2. Hence, no noticeable differences are found between the results computed with $Re \neq 0$ and those at the limit of creeping flow. Therefore, for fluids of viscosity greater than $0.01\,\mathrm{N\,s\,m^{-2}}$, electrohydrodynamic behaviour of leaky dielectric drops with prolate deformations can be reasonably described by models using the creeping-flow approximation.

Oblate drop deformations usually indicate relatively high flow intensity, because the oblate drop shape is necessarily maintained by the hydrodynamic stresses arising from the flow field against the normal electric stress that always tends to deform the drop into prolate shape (cf. Taylor 1966). For $\mathscr{S} = 2.0$ (i.e. $\kappa_o = 5$ and $\kappa_i = 2.5$) and $\mathscr{R} = 0.1$ with everything else unchanged as in obtaining (5.2), we have $Re = 2.041E^2$. Evaluated at $E = 0.7387$, the critical field strength for creeping flows, $Re \sim 1$; thus, inertial effects might emerge. Indeed, the critical field strength determined in this case with $Re \neq 0$ shows a slight change to $E_c = 0.7376$. Figure 6 shows both the comparative streamline pattern of flow fields, and the distributions of tangential surface velocity v_T along the drop interface for $Re = 1.10$ and $Re = 0$ at $E = 0.735$. The distribution of tangential surface velocity v_T is plotted versus the polar angle θ measured from the negative z-axis. The differences between the cases of $Re = 1.10$ and $Re = 0$ are in general too small to be noticeable in figure 6(*a*), except that the circulating eddy outside the drop is convected slightly upward for $Re = 1.10$ compared with that of $Re = 0$. The tangential surface velocity distribution for the case of $Re = 1.10$ (solid curve in figure 6*b*) also shows slight convection effects compared with that of $Re = 0$ (dashed curve in figure 6*b*). Reducing $\mathscr{R}$ from 0.1 to 0.01 leads to $Re = 2.729E^2$, only a slight increase in Re. Estimated at $E = 0.6040$, the critical field strength for creeping flows, we have $Re \sim 1.6$, and only a slight change of the critical field strength to $E_c = 0.6035$ is detected with corresponding $Re = 1.647$. Thus, as long as the viscosity of the fluids is greater than $0.01\,\mathrm{N\,s\,m^{-2}}$, electrohydrodynamic behaviour of leaky dielectric drops with oblate deformations can also be described with the creeping-flow approximation, even though Re may reach values of about unity.

5.2. *Cases with* $Re \sim O(10)$ *and* $\mathscr{S} = 0.5$

As expressed in (5.1), the value of Re is sensitive to the variation of viscosity μ_i and μ_o. For example, if $\mu = \mu_i = \mu_o$ varies by a factor of 10, Re should change by a factor of 10^2. Figure 7 shows both the comparative streamline pattern of flow fields and distributions of tangential surface velocity v_T along the drop interface for

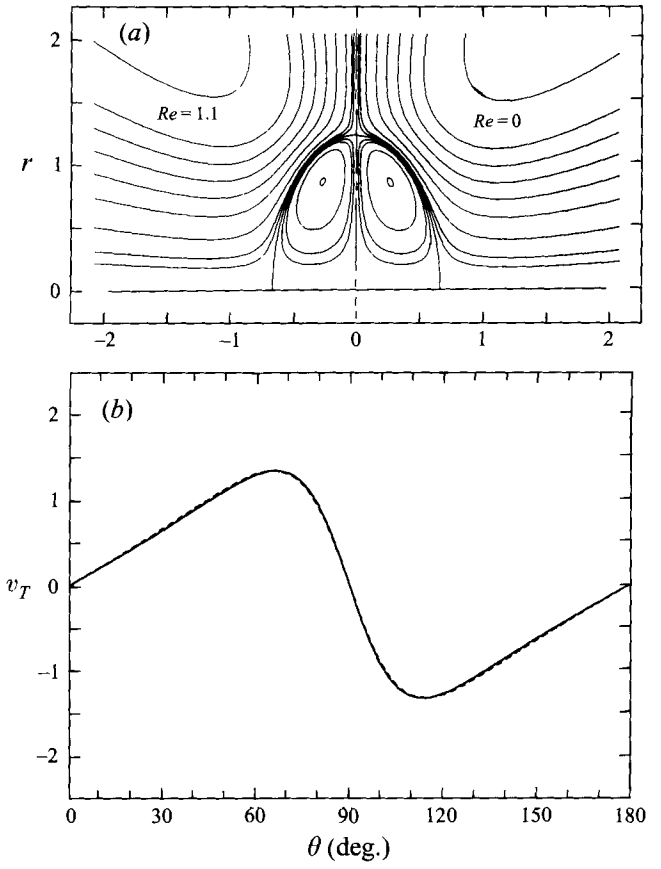

FIGURE 6. Comparison between electrohydrodynamic flows at finite Re and at $Re = 0$ with $\mu_i = \mu_o = 0.01\,\mathrm{N\,s\,m^{-2}}$, $\mathscr{R} = 0.1$, $\mathscr{S} = 2$, and $E = 0.735$. (*a*) Streamlines about a deformable drop with the streamline values chosen to be ± 0.01, ± 0.02, ± 0.05, ± 0.1, ± 0.15, ± 0.2, ± 0.25, ± 0.3, and ± 0.4. (*b*) Tangential surface velocity v_T versus polar angle θ: ——, $Re = 1.10$; - - - -, $Re = 0$.

$Re = 9.29$ and $Re = 0$ at $E = 0.3855$ with $\mu = 0.001\,\mathrm{N\,s\,m^{-2}}$, $\mathscr{S} = 0.5$, and $\mathscr{R} = 10$. Compared with that at $Re = 0$, the drop tends to be a little more elongated in the field direction with $Re = 9.29$, as shown in figure 7(*a*). The circulating eddy inside the drop shifts toward the pole slightly, and flow outside the drop exhibits more noticeable convection effects. The tangential surface velocity v_T distributions shown in figure 7(*b*) exhibit more significant convection effects with $Re = 9.29$ than that shown in figure 6(*b*). Although the critical field strength changes only slightly from $E_c = 0.3860$ at $Re = 0$ to $E_c = 0.3867$ at $Re = 9.35$, the deformation parameter D at critical field strength changes noticeably from $D_c = 0.4719$ at $Re = 0$ to $D_c = 0.5012$ at $Re = 9.35$, consistent with the more pronounced prolate deformation at finite Re.

With other parameters unchanged from those in figure 7, increasing $\mathscr{R}$ from 10 to 100 reduces the flow intensity, because (2.15) indicates that $U \to 0$ as $\mathscr{R} \to \infty$. The system is then expected to behave just like an uncharged conducting drop in an insulating fluid; it is again confirmed by our computation that there is no noticeable difference between the solutions at $Re = 0.916$ and $Re = 0$ when the critical field strength is approached. The value of the critical field strength hardly changes: $E_c = 0.2939$ at $Re = 0$ and $E_c = 0.2938$ at $Re = 0.916$. Furthermore, change in the

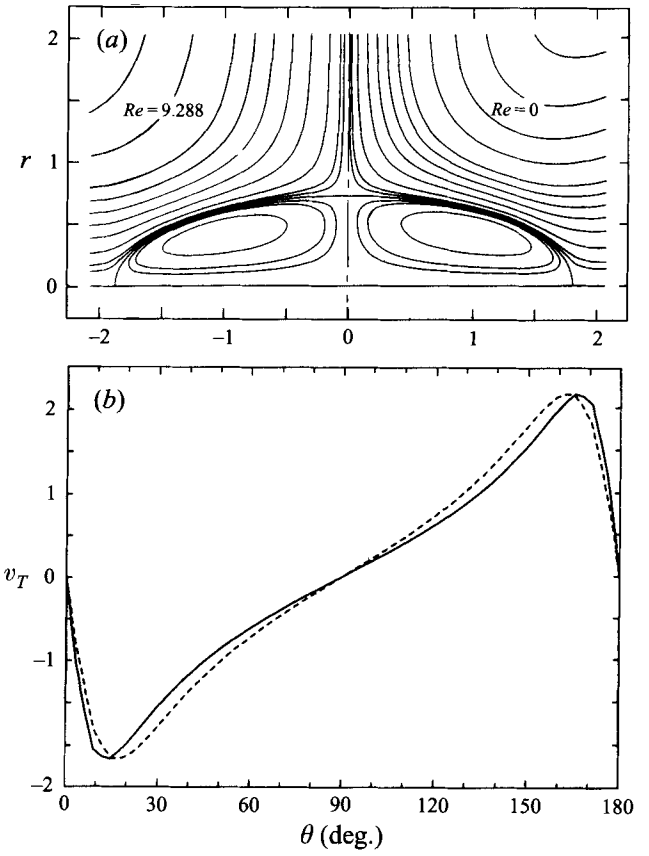

FIGURE 7. As figure 6 but with $\mu_i = \mu_o = 0.001\,\mathrm{N\,s\,m^{-2}}$, $\mathscr{R} = 10$, $\mathscr{S} = 0.5$, and $E = 0.3855$. In (*b*) ——, $Re = 9.288$; - - - -, at $Re = 0$.

deformation parameter D at critical field strength is also negligible: $D_c = 0.3035$ at $Re = 0$ and $D_c = 0.3059$ at $Re = 0.916$.

To increase the flow intensity, $\mathscr{R}$ is then reduced to 1.8123, keeping other parameters unchanged from those in figure 7. In this case Taylor's discriminating function (3.5) approaches zero and the drop shape retains sphericity at the limit of creeping flows. Figure 8(*a*) shows that for fluids with viscosity $\mu \sim 0.001\,\mathrm{N\,s\,m^{-2}}$, the drop exhibits mild prolate deformation at $E = 1$ with $Re = 28.18$. The flow field computed at finite Re also manifests some convection effects compared with that at $Re = 0$. The convection effects are more obvious in figure 8(*b*) for the tangential surface velocity v_T distributions. The deformation parameter evaluated at $E = 1$ with $Re = 28.18$ is $D = 2.52 \times 10^{-2}$, a significant increase from $D = 1.50 \times 10^{-4}$ as shown in table 1 at the limit of creeping flows. The loss of sphericity of a drop, in this case for a low-viscosity system, is definitely due to the finite-Re flow effects.

Although the value of Re can reach up to $O(10)$ for a system with $\mu = 0.001\,\mathrm{N\,s\,m^{-2}}$ and $\mathscr{S} = 0.5$, the electrohydrodynamic behaviour of leaky dielectric drops is altered only moderately. Hence, cases with larger Re must be investigated in order to detect dramatic changes at finite Re. On the other hand, our results computed with finite Re suggest that the generic features presented with the creeping-flow analysis in §4 are applicable to systems with a wide range of fluid property values.

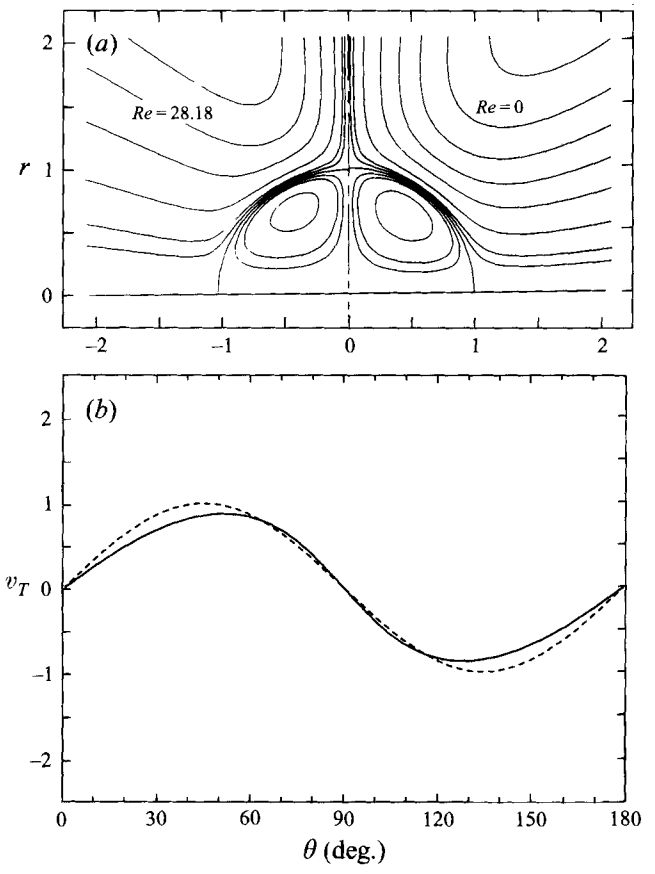

FIGURE 8. As figure 6 but with $\mu_i = \mu_o = 0.001\,\mathrm{N\,s\,m^{-2}}$, $\mathscr{R} = 1.8123$, $\mathscr{S} = 0.5$, and $E = 1$. In (*b*) ——, $Re = 28.18$; - - - -, $Re = 0$.

5.3. *Cases with* $Re \geqslant O(10)$ *and* $\mathscr{S} = 2.0$

For a system with $\mathscr{S} = 2.0$ and $\mathscr{R} = 0.3956$, creeping-flow solutions indicate that undeformed spherical drops can be maintained at arbitrarily large electric field strength for $\mathscr{M} = 1$. With $\mu = 0.001\,\mathrm{N\,s\,m^{-2}}$, Re takes a value of 40.95 at $E = 1$; therefore, the flow is unlikely to be the same as that described by the creeping-flow solution. In addition to convection effects exhibited in the flow field, the drop shape with $Re = 40.95$, shown in figure 9(*a*), deviates noticeably from sphericity toward a prolate spheroid. Evaluated at $E = 1$ with $Re = 40.95$, the drop deformation parameter is found to be $D = 4.44 \times 10^{-2}$, more than two orders of magnitude larger than $D = 1.50 \times 10^{-4}$ at the limit of creeping flow. Even though the fluid systems are quite different, the electrohydrodynamic behaviour seen in figure 9(*a*) is similar to that in figure 8(*a*). The distributions of tangential surface velocity v_T, shown in figures 8(*b*) and 9(*b*), suggest that the inertial effects at large Re tend to reduce the flow intensity. Less intensive flows give rise to weaker hydrodynamic stresses that are needed to maintain the drop sphericity against the prolate-inducing normal electric stress. Thus, drops consistently tend to be deformed into prolate shape with less intensive electrohydrodynamic flows as Re increases.

If $\mathscr{R}$ is reduced to 0.1 with other parameters unchanged from those corresponding

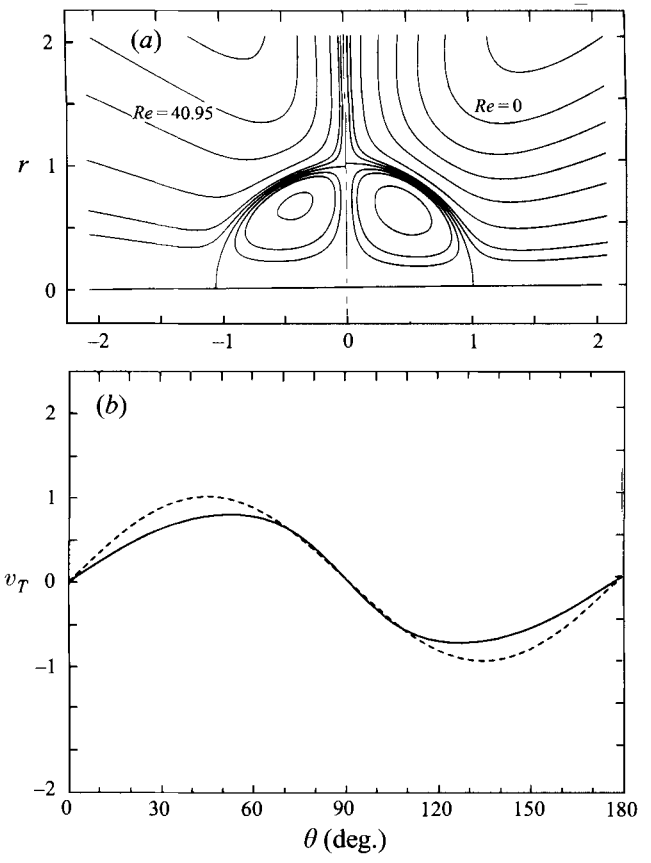

FIGURE 9. As figure 6 but with $\mu_i = \mu_o = 0.001\,\mathrm{N\,s\,m^{-2}}$, $\mathscr{R} = 0.3956$, $\mathscr{S} = 2$, and $E = 1$. In (*b*) ——, $Re = 40.95$; - - - -, $Re = 0$.

to figure 9, we have $\Phi < 0$ and drops are expected to exhibit oblate deformations, according to the asymptotic theory with the creeping-flow approximation. With $\mu = 0.001\,\mathrm{N\,s\,m^{-2}}$, however, Re can become as large as 204.08 if E reaches 1. The tendency toward prolate drop deformation when Re becomes large, however, indicates subtle variations in electrohydrodynamic drop deformations with increasing E. Indeed, the computational results show a remarkable phenomenon of drop shape turnaround from oblate deformation at low electric field strength to prolate-like deformation at the high field strength, as shown in figure 10. At low electric field strength $E = 0.1$, the drop is nearly spherical. The oblate deformation emerges as E is increased somewhat, following the trend shown by the solutions with the creeping-flow restriction. Then, with further increase of E, maximum oblate deformation is reached at $E = 0.401$. Thereafter, increasing E reduces the oblate deformation, and at $E = 0.6447$ the absolute value of D diminishes. However, the drop shape with $D \sim 0$ is not quite spherical; rather its profile contains a small component of the diamond shape. Increasing E even further results in an elongation of the drop in the field direction. At $E = 1$, we have $Re = 204.08$. Although D takes a positive value, the drop shape cannot be well described by a prolate spheroid because the drop surface bulges at the equator while the poles are stretched away from each other. The drop shape actually consists of significant numbers of higher-degree components of the

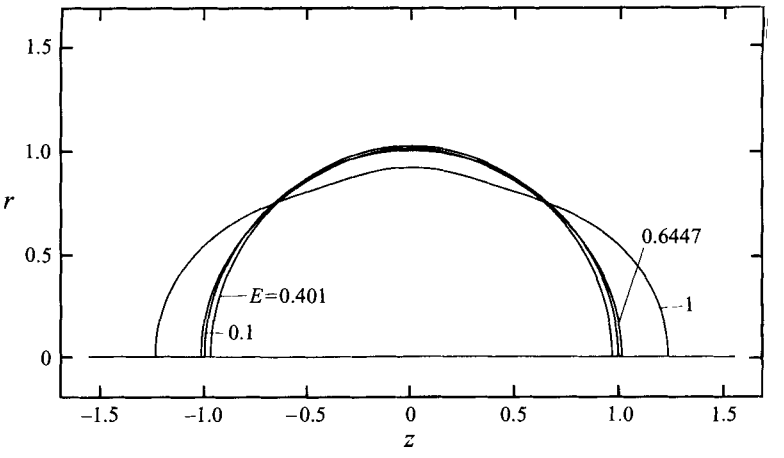

FIGURE 10. Variation of drop shape with E when $\mathscr{R} = 0.1$, $\mathscr{S} = 2$, and $\mu_i = \mu_o = 0.001\,\mathrm{N\,s\,m^{-2}}$. The deformation parameter D takes values −0.00366, −0.0291, 0, and 0.145 at $E = 0.1$, 0.401, 0.6447, and 1, respectively.

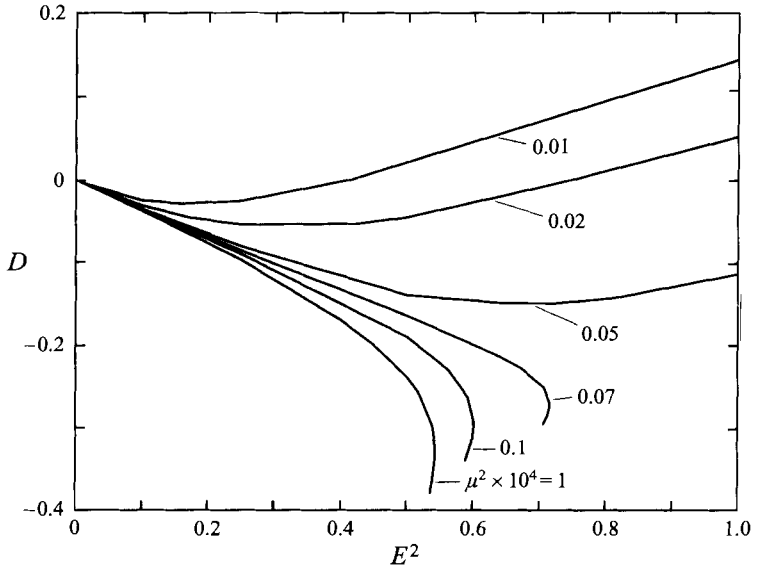

FIGURE 11. Steady-state solution branches of families in the parameter space of D as a function of E^2 for $\mathscr{R} = 0.1$ with $\mathscr{S} = 2$ and various values of μ^2 where $\mu = \mu_i = \mu_o$.

Legendre polynomials, especially P_4, in addition to P_2 and P_0 for the oblate–prolate type deformations.

The parameter-space plot of D versus E^2 in figure 11 provides an overview of the evolution of drop deformations for various values of viscosity μ with $\mathscr{R} = 0.1$ and $\mathscr{S} = 2$. Roughly speaking, there is a transition zone bordered by the curves corresponding to $\mu^2 \times 10^4 = 0.05$ and 0.07 with μ in units of $\mathrm{N\,s\,m^{-2}}$, wherein the behaviour of the solution branch switches from the normal increase in the oblate deformation with E^2 and folds back at a turning point to the drop shape turnaround from oblate deformations at small E to prolate-like deformations at large E. When

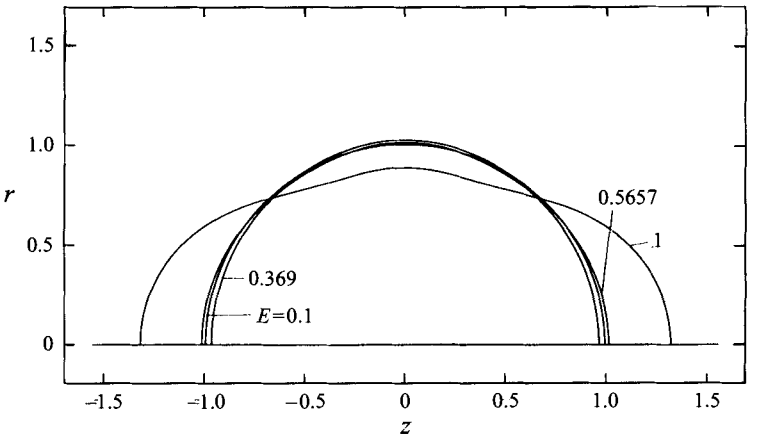

FIGURE 12. Variation of drop shape with E when $\mathscr{R} = 0.01$, $\mathscr{S} = 2$, and $\mu_i = \mu_o = 0.001\,\mathrm{N\,s\,m^{-2}}$. The deformation parameter D takes values −0.00490, −0.0305, 0, and 0.196 at $E = 0.1$, 0.369, 0.5657, and 1, respectively.

the value of μ is reduced, the critical field strength E_c at the turning point increases and, correspondingly, drops exhibit less pronounced oblate deformation at a given E. Although not precisely determined here, a critical value of $\mu^2 \times 10^4$ clearly exists in the interval (0.05, 0.07) below which there is no turning point to be encountered by any solution branches. The solution branches without turning points exhibit the drop shape turnaround phenomenon. At small values of E, the electrohydrodynamic flow is weak and Re is small. Therefore, the drop behaviour is essentially described by the creeping-flow solutions with the oblate deformation. With increasing E, the value of Re increases and the drop behaviour deviates from that described by the creeping-flow solutions. Hence, the maximum oblate deformation is reached at finite values of E, while the oblate deformations are then alleviated with further increase of E. Eventually, drops are deformed into prolate-like shapes at large E, as is consistent with the general trend of drop behaviour at large Re.

Reducing $\mathscr{R}$ from 0.1 to 0.01 is expected to enhance the flow intensity somewhat. Shown in figure 12 are a few representative drop shapes, which exhibit behaviour quite similar to that seen in figure 10, except that the maximum oblate deformation now happens at $E = 0.369$ and the deformation parameter D approaches zero at $E = 0.5657$. In addition, the prolate-like drop deformation is also more pronounced at $E = 1$. Just as in figure 11, the solution branches in the parameter space of D versus E^2 in figure 13 for $\mathscr{R} = 0.01$ also manifest two different behaviours: folding back at turning points and drop shape turnaround from oblate to prolate-like deformations. Although the variation of D seems to be more sensitive to E^2 when $\mathscr{R} = 0.01$ than with the corresponding value of μ when $\mathscr{R} = 0.1$, the transition zone wherein the solution branches switch qualitative behaviour is still bordered by the curves corresponding to $\mu^2 \times 10^4 = 0.05$ and 0.07, with μ in units of $\mathrm{N\,s\,m^{-2}}$.

According to the present computational results, the phenomenon of drop shape turn-around occurs only in systems with low-viscosity fluids where Re can reach large values. Interestingly, the phenomenon of a drop with oblate deformation at low E eventually turning into a prolate shape with increasing E was also reported by Vizika & Saville (1992) under a totally different mechanism that seemed to result from the

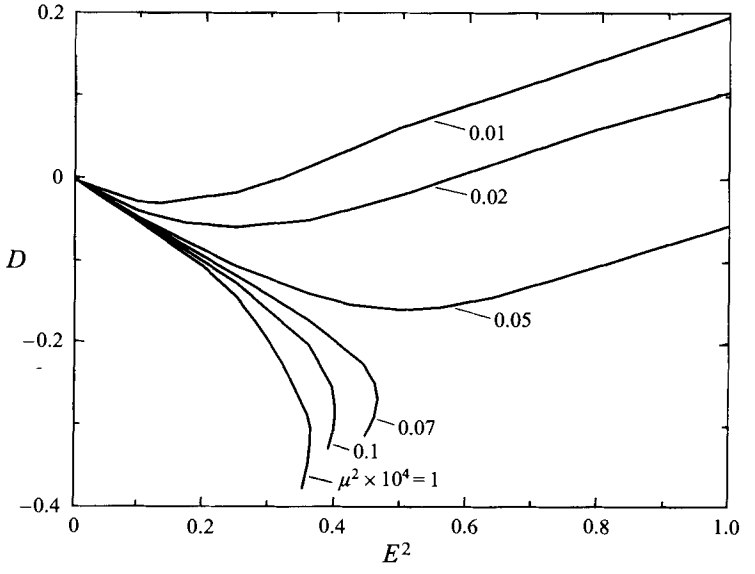

FIGURE 13. Steady-state solution branches of families in the parameter space of D as a function of E^2 for $\mathscr{R} = 0.01$ with $\mathscr{S} = 2$ and various values of μ^2 where $\mu = \mu_i = \mu_o$.

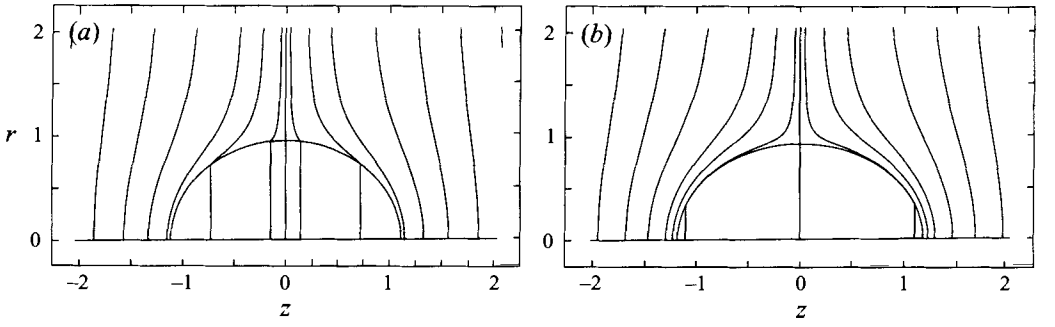

FIGURE 14. Equipotentials of electric field about a deformable drop at $\mu_i = \mu_o = 0.01\,\mathrm{N\,s\,m^{-2}}$, $\mathscr{S} = 0.5$, and $E = 0.25$, for (*a*) $\mathscr{R} = 10$ and (*b*) $\mathscr{R} = 100$. For illustrative purposes, the equipotential values are chosen to be 0, ± 0.01, ± 0.05, ± 0.1, ± 0.2, ± 0.3, ± 0.4, and ± 0.5.

variation of liquid conductivity with E. In their experiments, all systems involve very viscous liquids, and only creeping flows at very low Re could be generated.

6. Electric field distribution

Because electrohydrodynamics involve both the electric field and flow field, the distribution of electric field around the leaky dielectric drops is of fundamental interest. Figure 14 shows the equipotential contours, i.e. the contours of constant values of electric potential, around the prolate drops in systems with $\mathscr{S} = 0.5$ and $\mu = 0.01\,\mathrm{N\,s\,m^{-2}}$ for $\mathscr{R} = 10$ and 100. In the case of $\mathscr{R} = 10$, the drop interface does not quite conform to any equipotential contours, and substantial electric field exists inside the drop (see figure 14*a*), because the charges accumulated on the interface are

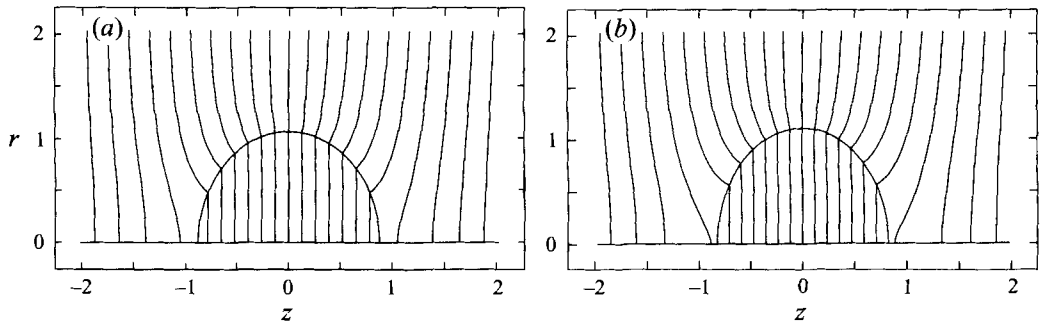

FIGURE 15. Equipotentials of electric field about a deformable drop at $\mu_i = \mu_o = 0.01\,\mathrm{N\,s\,m^{-2}}$, $\mathscr{S} = 2$, and $E = 0.5$, for (*a*) $\mathscr{R} = 0.1$ and (*b*) $\mathscr{R} = 0.01$. The equipotential values are 0, ± 0.1, ± 0.2, ± 0.3, ± 0.4, ± 0.5, ± 0.6, ± 0.7, ± 0.8, ± 0.9, and ± 1.

contributed from both inside and outside the drop, with a relatively small conductivity difference. If $\mathscr{R}$ is increased to 100, the interior fluid is much more conductive than the exterior one, and the drop surface approaches an equipotential state, as shown in figure 14(*b*). At a given field strength, because the net electric stresses at the drop interface are determined by the field strength difference on the two sides (see e.g. (2.8) and (2.9)), a drop in the system with $\mathscr{R} = 10$ is subjected to relatively weak electric stresses and therefore is deformed less than the one in the system with $\mathscr{R} = 100$.

The equipotential contours around the oblate drops in systems of $\mathscr{S} = 2.0$ and $\mu = 0.01\,\mathrm{N\,s\,m^{-2}}$ with $\mathscr{R} = 0.1$ and 0.01 are shown in figure 15. For those systems with $\mathscr{R} < 1$, the fluid outside the drop is relatively more conductive and the electric field strength is higher inside the drop. A drop in the system with $\mathscr{R} = 0.1$ (see figure 15*a*) is deformed less than that in the system with $\mathscr{R} = 0.01$ (see figure 15*b*) at a given electric field strength.

Noteworthy here is that the cases shown in figure 15 represent merely the inverse systems of those shown in figure 14. Hence, dramatically different electrohydrodynamic behaviour can be obtained by simply inverting the system, namely, by turning the inside phase out, a fact also observed in the numerical results obtained by Tsukada *et al.* (1993). With a more conductive fluid outside the drop, a much stronger gradient of electric potential is generated along the drop interface. From the expression of the Maxwell stress tensor (2.9), the tangential electric stress at the drop interface that drives the electrohydrodynamic flow is determined by the product of the tangential and normal components of the local electric field. Physically, the normal component of electric field that changes abruptly (or jumps) at the interface corresponds to the net surface charge accumulation, whereas the tangential electric field acts upon the charges at the interface to generate the shear stress that drags the fluid into motion. Hence, significant electrohydrodynamic flows are expected to occur in a two-phase fluid system if it is arranged so that the more conductive fluid serves as the continuous phase. This fact may be quantitatively illustrated by examining the value of

$$\frac{U}{E^2} \equiv \frac{9|\mathscr{S}\mathscr{R} - 1|}{10(2+\mathscr{R})^2(1+\mathscr{M})} \frac{\kappa_i \gamma}{\mu_i} \quad (\mathrm{m\,s^{-1}}), \tag{6.1}$$

which represents the normalized intensity of flow induced by the electric driving force.

Table 4 shows the variation of the value of UE^{-2} with $\mathscr{R}$ at $\mathscr{S} = 0.5$ with $\kappa_o = 2.5$ and at $\mathscr{S} = 2$ with $\kappa_o = 5$ for $\mu = \mu_o = \mu_i = 0.01\,\mathrm{N\,s\,m^{-2}}$ and $\gamma = 0.001\,\mathrm{N\,m^{-1}}$. As expected, the flow intensity decreases as $\mathscr{R}$ increases for a given value of E. When

$\mathscr{S}$	$\mathscr{R}$	UE^{-2} ($m\,s^{-1}$)
0.5	10	6.25×10^{-3}
0.5	100	1.06×10^{-3}
0.5	1000	1.12×10^{-4}
0.5	∞	0
2	0.1	2.04×10^{-2}
2	0.01	2.73×10^{-2}
2	0.001	2.80×10^{-2}
2	0	2.81×10^{-2}

TABLE 4. Variations of value of UE^{-2} with $\mathscr{R}$.

the drop is more conductive than the surrounding fluid, the flow intensity decreases at a rate $\sim 1/\mathscr{R}$ for $\mathscr{R} > 100$. If the surrounding fluid is more conductive than that inside the drop, however, the flow intensity becomes insensitive to the variation of $\mathscr{R}$. Thus, the contrast of conductivities in a system with more conductive surrounding fluid is not expected to significantly affect the electrohydrodynamic flow intensity. However, some overall electrohydrodynamic behaviour of drops, such as the critical electric field strength and drop deformations, can still be influenced by the value of $\mathscr{R}$ through the change in electric field distribution.

7. Comparison with experimental data

From the data presented by Torza *et al.* (1971) and Vizika & Saville (1992), we found that all experiments were conducted with systems involving liquids that are much more viscous than water. Even for the cases where drops of distilled water were used, the viscosities of the liquids used as the surrounding phase were so large that the values of $\mathscr{M}$ always became greater than 10^3. The highly viscous liquids were preferred as the surrounding fluid in the experiments, because they hinder the undesirable migration of drops due to slight imbalance of forces. Therefore, all the available experimental information was obtained from systems that are expected to be well described by the theory at the limit of creeping flow. The experiments recently reported by Tsukada *et al.* (1993) also correspond to low-Reynolds-number flows; therefore, their computations were actually restricted to the limit situation of creeping flow.

As presented in §4.2 for the creeping-flow situations, the solution branches in the parameter space D versus E^2 usually display an increase in both $|D|$ and $|\mathrm{d}D/\mathrm{d}(E^2)|$ with E^2 up to the point at which the turning points are reached. The corresponding asymptotic lines with constant $\mathrm{d}D/\mathrm{d}(E^2)$ often underestimate the deformation parameter D for those systems formed in the experiments. The discrepancy between the computational results (solid curves) and those predicted by the asymptotic theory (dashed lines) is negligible when $|D|$ is small, e.g. $D < 0.05$ for prolates and $D > -0.1$ for oblates; it becomes noticeable when $|D|$ exceeds 0.1 and increases significantly thereafter. In general, the discrepancies for prolate deformations are greater than those for oblate deformations. According to the computational results, the experimental data obtained with a given system should inherently follow a nonlinear relationship between D and E^2. Discrepancy is almost inevitable when the data are fitted to a straight line and then compared with the corresponding asymptotic line.

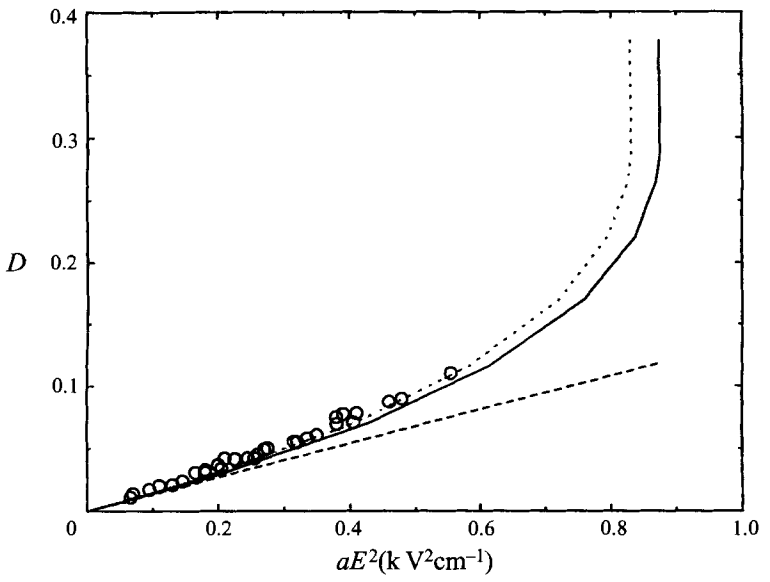

FIGURE 16. Comparison between theory and experiment for the case of a water drop in castor oil: ——, computational results; - - - -, prediction of asymptotic theory; ·····, computations with 5% reduction of γ; and ○, experimental data.

A qualitative explanation for the significant discrepancy between experimental measurements reported by Torza *et al.* (1971) and Taylor's asymptotic theory (1966) might be that most of the experimental data were acquired at large E close to the critical field strength E_c. Based on our results given in table 2, $|D_c|$ can usually be greater than $|D_a|$ by a factor of two to three. On the other hand, the improved agreement between Taylor's asymptotic theory and experiment found by Vizika & Saville (1992) might then be naturally explained by the fact that most of their experimental data were acquired at values of E much lower than the critical field strength, and therefore $|D|$ was kept small. Indeed, the data points shown in figure 7 of the paper by Vizika & Saville (1992) for the deformation measurements in oscillatory fields fall mostly within the regime of $|D_s| < 0.05$, and excellent agreement was found there with the asymptotic theory.

In this section, we compare our computational results and those representative raw data points shown by Vizika & Saville (1992) for steady-field cases. Following the convention established by previous authors, we use E to denote the dimensional strength of the applied electric field in units of k V cm^{-1}, unless otherwise specified. The abscissa in the plots below then represents aE^2 in units of k V^2 cm^{-1}, as calculated by multiplying our dimensionless E^2 by $10^{-8}\gamma/\epsilon_0$. Only a limited number of raw data points can be found in the paper by Torza *et al.* (1971), although they measured the slopes $\mathrm{d}D/\mathrm{d}(aE^2)$ for a large number of systems. This restricts our direct comparison with their experimental results to only a couple of cases. A comparison of two sets of experimental data was presented by Tsukada *et al.* (1993), along with their own numerical solutions, which is unnecessary to repeat here.

7.1. *Cases of prolate drops*

Figure 16 shows the plot of D versus aE^2(k V^2 cm^{-1}) for the case of a water drop in castor oil. According to the data given by Vizika & Saville (1992), we have

$\mathscr{S} = 0.057$ with $\kappa_o = 4.45$, $\mathscr{M} = 1400$ with $\mu_o = 1.4\,\mathrm{N\,s\,m^{-2}}$, and $\gamma = 0.0168\,\mathrm{N\,m^{-1}}$. None of the exact values for $\mathscr{R}$ were given by Vizika & Saville (1992); they simply put $\mathscr{R} > 10^4$ for this system in a table. We choose a value of $\mathscr{R} = 1500$ for the convenience of computations; the value so chosen is not expected to make any difference in the computational results, as we discussed previously. As expected, the experimental data for this case deviate from the (dashed) asymptotic line in the same direction as the (solid) computational curve does and, therefore, agree quite well with the computational results. Yet, consistently, most experimental data points are still located slightly above the solid computational curve. By simply reducing the value of interfacial tension γ by 5%, as also shown in figure 16 with the dotted curve, the agreement between the computational curve and experimental data becomes almost perfect. In contrast, a more than 25% reduction of the interfacial tension would be needed to bring the asymptotic line to reasonably fit the experimental data for this case. The accuracy of interfacial tension measurements is not clearly stated in the literature. Therefore, at this point, only suggestions can be made based on the present observation.

Just like the system shown in figure 16, many experiments with prolate drops were conducted with systems in which a much more conducting drop in a relatively insulating fluid (i.e. $\mathscr{R} > 10^4$) was subjected to an electric field, which corresponds to a generic electrohydrostatic situation. Theoretically, the behaviour of these systems can be well described by one solution branch in terms of a dimensionless parameter $\kappa_o E^2$, with E now denoting the dimensionless field strength as defined in §2. Indeed, as shown in figure 17, computational curves for three different experimental systems fall on top of each other when converted to the dimensionless plot of D versus $\kappa_o E^2$. Scattered around the computational curve are the relevant experimental data points, including those shown in figure 16 and three additional sets of data that are also found in figure 5 of the paper by Vizika & Saville (1992). These three additional experimental systems correspond to a water drop in silicone oil (300 P) (where $\mathscr{S} = 0.035$ with $\kappa_o = 2.75$, $\mathscr{M} = 3 \times 10^4$ with $\mu_o = 30\,\mathrm{N\,s\,m^{-2}}$, and $\gamma = 0.0283\,\mathrm{N\,m^{-1}}$), a drop of water + Triton in silicone oil (125P) (where $\mathscr{S} = 0.035$ with $\kappa_o = 2.75$, $\mathscr{M} = 357$ with $\mu_o = 12.5\,\mathrm{N\,s\,m^{-2}}$, and $\gamma = 0.00425\,\mathrm{N\,m^{-1}}$), and a drop of water + Triton in castor oil (where $\mathscr{S} = 0.057$ with $\kappa_o = 4.45$, $\mathscr{M} = 40$ with $\mu_o = 1.4\,\mathrm{N\,s\,m^{-2}}$, and $\gamma = 0.0015\,\mathrm{N\,m^{-1}}$). Most experimental data points are located above the asymptotic line and are better represented by the computational curve, except for the data set for a drop of water + Triton in silicone oil (125 P), which shows remarkable agreement with the asymptotic line. Theoretically, the asymptotic line cannot be very accurate when the deformation parameter D exceeds the value 0.05. If this were attributed to the error in the measurement of interfacial tension, an increase in the value of interfacial tension by about 20% would be needed to bring the data to fit the computational curve. As a side note, if averaging is taken over all the data points across the different systems, a fortuitous agreement occurs between experiments and the computational results. The theory shows that the differences in the liquid properties between these different systems should not affect the experimental results in the non-dimensional parameter space, as long as the conductivity ratio $\mathscr{R} > 100$. The finding that agreement between the theory and experiment improves by averaging across various systems suggests the cancellation of some system errors such as different interfacial tension measurements obtained for different systems.

According to the computational results shown in this work, the drop behaviour in the systems with large values of $\mathscr{R}$ is actually well described by the electrohydrostatic theory, which deals with no fluid flows. This finding is consistent with (2.15), which

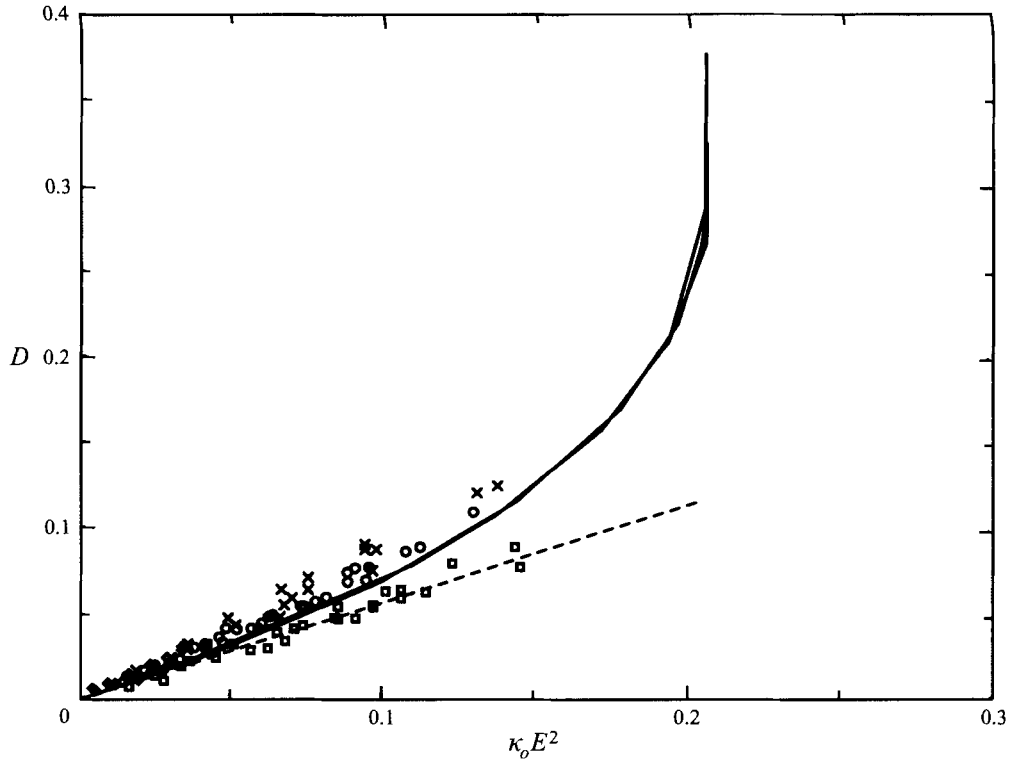

FIGURE 17. Comparison between theory and experiment in the non-dimensional parameter space of D versus $\kappa_o E^2$ for the extreme case of large $\mathscr{R}$: ——, indicates computational results; - - - -, prediction of asymptotic theory; and ○, ◇, □, ×, experimental data for the cases of a water drop in castor oil, a water drop in silicone oil (300 P), a water + Triton drop in silicone oil (125 P), and a water + Triton drop in castor oil, respectively.

suggests vanishing characteristic velocity as $\mathscr{R} \to \infty$. It is interesting to note that the experiments with the systems of $\mathscr{R} > 10^4$ e.g. those shown in figures 16 and 17 along with others published by Torza *et al.* (1971) and Vizika & Saville (1992), were conducted to investigate the electrohydrodynamic behaviour of drops. All the experimental data were fitted to straight lines for the comparison with that predicted by the asymptotic electrohydrodynamic theory of Taylor (1966), while the more relevant electrohydrostatic theory of Taylor (1964), which clearly indicates the existence of critical field strength and the general nonlinear behaviour of the solution branches in the parameter space, was not considered.

As an exception to the extreme situation shown in figure 17, the experimental data set found in figure 6 of the paper by Torza *et al.* (1971) for a drop of castor oil in silicone oil is examined here. In this system, $\mathscr{S} = 0.44$ with $\kappa_o = 2.77$, $\mathscr{M} = 0.83$ with $\mu_o = 5.4\,\mathrm{N\,s\,m^{-2}}$, and $\gamma = 0.0055\,\mathrm{N\,m^{-1}}$. The conductivity ratio is given as $\mathscr{R} > 30$, and we simply use $\mathscr{R} = 30$ for our computations. Figure 18 shows the computational curve and experimental data for this particular case in terms of dimensional parameter $aE^2(\mathrm{k\,V^2\,cm^{-1}})$, as used in figure 16. Again, the nonlinear relationship of D and aE^2 predicted by the computational (solid) curve matches the experimental data much better than the asymptotic (dashed) line.

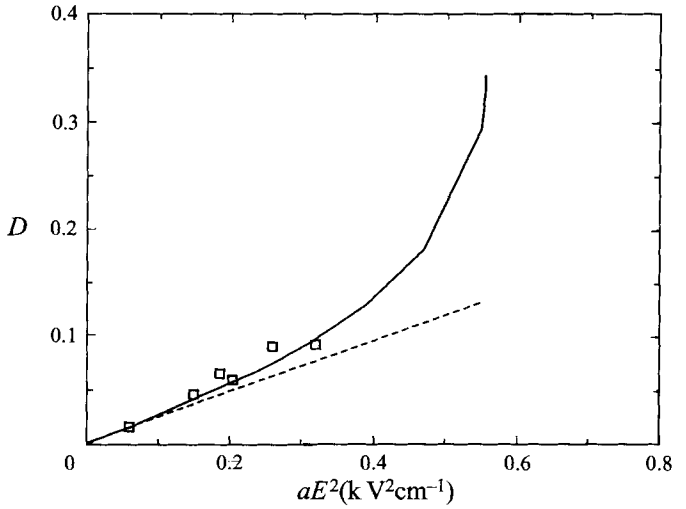

FIGURE 18. Comparison between theory and experiment for the case of a castor oil drop in silicone oil: ——, computational results; - - - -, prediction of asymptotic theory; and □, experimental data.

7.2. *Cases of oblate drops*

Not many raw experimental data can be found in the literature for the oblate drops. Vizika & Saville (1992) presented two cases in figure 6 of their paper. However, one of those cases behaved abnormally owing to problems with controlling the liquid conductivity. Here we compare our computations with the normal one, which was apparently free from system problems. This is the case of a drop of silicone oil (125 P) in castor oil + Triton, where $\mathscr{S} = 2.04$ with $\kappa_o = 5.6$, $\mathscr{M} = 0.08$ with $\mu_o = 1.0\,\mathrm{N\,s\,m^{-2}}$, and $\gamma = 0.00425\,\mathrm{N\,m^{-1}}$. Because $\mathscr{R} < 10^{-4}$ was given for this system, a value of $\mathscr{R} = 0.001$ is chosen for the computations. The results are presented in figure 19(*a*). The experimental data show slightly less pronounced drop deformations than that predicted by the (dashed) asymptotic line. The only situations with very low *Re* where the computational results show less pronounced drop deformations than the asymptotic prediction have been found in §4 when the values of conductivities become very close, i.e. $\mathscr{R} \sim O(1)$. For the present case where $\mathscr{R} < 10^{-4}$, the computational curve consistently predicts greater drop deformations than the asymptotic theory. Within the region covering the data set, however, the differences among the computational results, the experimental data, and the asymptotic line remain small. Therefore, the agreement between theory and experiment appears to be reasonably good.

Another data set for oblate drops is found in figure 6 of the paper by Torza *et al.* (1971) for a drop of silicone oil in castor oil – merely an inverted system from that shown in figure 18. For this case, $\mathscr{S} = 2.274$ with $\kappa_o = 6.3$, $\mathscr{M} = 1.204$ with $\mu_o = 6.5\,\mathrm{N\,s\,m^{-2}}$, and of course $\gamma = 0.0055\,\mathrm{N\,m^{-1}}$. The conductivity ratio is then given as $\mathscr{R} < 0.0333$, and we simply use $\mathscr{R} = 0.0333$ for our computations. Figure 19(*b*) shows that for this case the experimental data consistently represent greater oblate deformations than those predicted by both the (solid) computational curve and (dashed) asymptotic line. Although the computational curve tends to bend away from the asymptotic line toward greater drop deformations with increasing electric field strength, it does not go far enough to completely fit the experimental data in the region where the data points appear. All that can be said is that the computational curve indeed suggests the general trend of greater oblate deformations

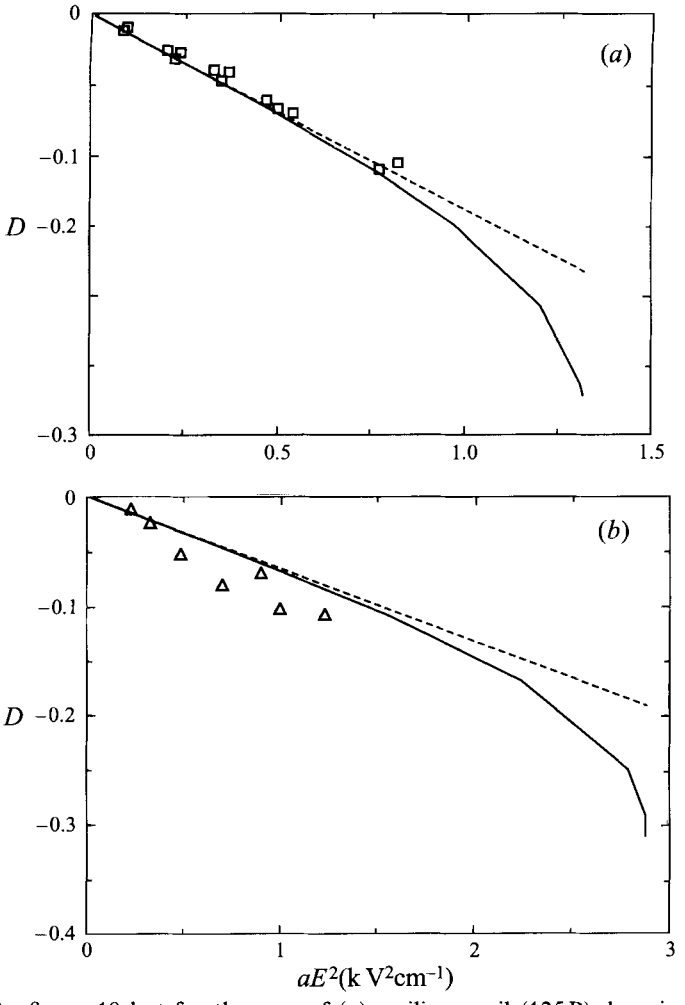

FIGURE 19. As figure 18 but for the case of (*a*) a silicone oil (125 P) drop in castor oil + Triton, (*b*) a silicone oil drop in castor oil: ——, computational results; - - - -, prediction of asymptotic theory; and □, △, experimental data.

shown by this set of experimental measurements. Of course, the agreement can be improved by reducing the value of interfacial tension.

8. Concluding remarks

By means of the Galerkin finite-element method, the nonlinear free-boundary problem of electrohydrodynamics of a neutrally buoyant drop in an immiscible fluid subjected to an electric field is solved numerically within the framework of the leaky dielectric model. Excellent agreement between the numerical solutions and the asymptotic solutions of Taylor (1966) for creeping flow around nearly spherical drops has been found when both the Reynolds number *Re* and drop deformations from the spherical shape are small. Significant differences between the computational prediction and that of the asymptotic theory have been revealed when the drop deformations become noticeable, even in the limit of creeping flows. It has been shown computationally that the solution branches, represented in the parameter

space of the drop deformation parameter D versus the square of the dimensionless strength of electric field E, usually deviate from the corresponding asymptotic lines toward larger deformations with the slopes $|\mathrm{d}D/\mathrm{d}(E^2)|$ also increasing with E^2.

Critical field strength E_c at mathematical turning points in the parameter space has been determined computationally with an arc-length continuation method. Physically, those turning points signal the stability limits of drops stressed by an electric field (Iooss & Joseph 1990; Ungar & Brown 1982). No steady solution can be obtained locally if the externally applied electric field is increased beyond the critical field strength. The solution branches fold back at the turning points to lower values of the field strength, and thereby more than one steady solution exists for a given field strength $E < E_c$. Solution branches folding back at turning points have been commonly found in the electrohydrostatic analyses of electrified drop systems, where either both fluids are regarded as perfectly insulating or the drop is considered to be highly conducting with a perfectly insulating fluid outside (cf. Garton & Krasucki 1964; Taylor 1964; Rosenkilde 1969; Miksis 1981; Adornato & Brown 1983; Basaran & Scriven 1989). The similar behaviour in the electrohydrodynamic situation of leaky dielectric drops has not been explicitly discussed until the present work. The computational results presented here show that the solution branches representing both prolate and oblate drops can encounter turning points in the parameter space.

Much like the situation of a dielectric drop in an insulating fluid with a small difference between the inside and outside dielectric constants, some solution branches of leaky dielectric drop systems, especially those with small differences between the inside and outside conductivities, have been found to indicate drop deformations growing indefinitely with the electric field strength without encountering turning points. A similar phenomenon of drop deformation smoothly increasing with electric field strength was also shown by Sherwood (1988) for the case with relatively small differences in both dielectric constants and conductivities. In some special situations, the computationally determined solution branches appear to almost coincide with those predicted by the asymptotic theory even at large electric field strength. Because many parameters in the present mathematical system can influence the electrohydrodynamic behaviour, exploration of all possible categories of solution branches in various parameter spaces demands quite involved work and is not pursued in this paper.

By virtue of the generality of the Galerkin finite-element scheme used in this work, electrohydrodynamic flows at finite Reynolds number Re have also been investigated. For most liquid–liquid systems, the inertial effects that come with the flows at finite Re alter the electrohydrodynamic behaviour moderately from that in the creeping-flow situation. If the viscosities of both the fluids inside and outside of the drop are reduced to the level of that of water, however, our computations have predicted a dramatic change in the electrohydrodynamic behaviour: certain solution branches that correspond to oblate drop deformations at low Re turn around at finite values of E with fairly large values of Re toward prolate-like drop deformations with increasing E. A general tendency seems to exist for the drops with electrohydrodynamic flows of large Re to be deformed into prolate-like shapes. This tendency toward prolate-like drop deformations has also been exhibited at large Re in the systems where the drops are expected to remain spherical at arbitrarily large E, according to the results with the creeping-flow approximation.

All solutions obtained in this work correspond to symmetric drop shapes with respect to the equatorial plane, although the mathematical system is set up to be

general enough to allow the asymmetric shapes to be computed. Still, this does not mean that the possible existence of the asymmetric shapes should be excluded. As is usually true of nonlinear systems, surprising phenomena may be detected when new regions in parameter space are explored, because of the lack of general mathematical solutions. Detecting asymmetric shapes of steady drops with electrohydrodynamic flows may become an interesting subject for future research.

All liquid–liquid systems used in the experiments so far involve large viscosities, and only low-Reynolds-number flows can be generated (Torza *et al.* 1971; Vizika & Saville 1992; Tsukada *et al.* 1993). Accordingly, the present computational findings with flows at relatively large Re have to await future experimental verification. At present, only those computational results that correspond to creeping flows can be compared with experiments. The nonlinear relationship between D and E^2 revealed by the computations appears to be capable of explaining most discrepancies between the experiment and asymptotic theory reported in the literature. Strictly speaking, most experimental data should follow the nonlinear curves in the parameter space of D versus E^2 rather than the asymptotic line. Discrepancy is inevitable if one attempts to fit experimental data to a straight line and then to compare it with the asymptotic line.

The computational analysis presented here suggests that future experimental study should focus on measurements of large drop deformations (e.g. $D \geqslant 0.1$) because the deviation from the asymptotic line and the nonlinear relationship between D and E^2 are expected to become obvious. In addition to verifying theoretical prediction, the measurements of critical field strength and the corresponding drop deformations may provide accurate information for identifying errors in the experimental procedures. Theoretically, with charge convection effects neglected, only the conductivity ratio $\mathscr{R}$ can influence the electrohydrodynamic behaviour of drops, while the absolute values of the conductivities have no role to play. For those systems where one fluid is much more conductive than the other, accurate measurements of conductivities are unnecessary, because it is computationally shown that the electrohydrodynamic behaviour becomes insensitive to the actual value of $\mathscr{R}$ when one fluid is more conductive than the other by a factor of 10^2. The values of dielectric constants and interfacial tension, however, can easily affect the location of the data points in the parameter space. To observe significant electrohydrodynamic flow effects, systems with the outer phase more conductive than the inner phase are preferred, especially with drops exhibiting oblate deformations. As also suggested by Vizika & Saville (1992), experiments with a wider range of fluid properties are useful to further verify the theory based on the leaky dielectric model.

The present work extends Taylor's (1966) linear asymptotic results to include nonlinearities arising from large drop deformations and finite fluid inertial effects. In our work, only essential physical mechanisms that allow tangential electric stress to appear for driving electrohydrodynamic flows are considered. Without including other complications, the present mathematical system and the theoretical results derived therefrom are self-consistent. However, some additional physical mechanisms may also influence the experimental results for electrohydrodynamic behaviour of leaky dielectric drops, as suggested by previous investigators (cf. Vizika & Saville 1992). Among others, the effects of charge convection at the drop interface may be included as a natural extension of the present work. Because no sources of net charge can be traced along a particle path line in the present problem, charge convection by flow field naturally disappears in the bulk region (cf. Melcher 1981). Only at the drop interface may charge convection by fluid flow become effective. Without actually

obtaining the final mathematical solution, Torza *et al.* (1971) examined theoretically the convection of charge at the interface and concluded that such effects could not play an important role in their experiments. Vizika & Saville (1992) also found no obvious evidence of charge convection effects. All these previous investigators studied charge convection based on qualitative considerations; quantitative investigation, which relies on the solution of a nonlinear mathematical system, is difficult with the conventional mathematical tools. The computational scheme described in this work appears to be quite suitable for such a nonlinear analysis. Therefore, the effects of charge convection should be added to the list of future research subjects in the area of leaky dielectric drops. Moreover, including charge convection may provide better opportunities for asymmetric drop shapes with respect to the equatorial plane to appear because of additional nonlinearities.

Within the present mathematical framework, thorough theoretical analysis is in principle enabled by the numerical scheme described herein. However, the large set of parameters involved in the present problem makes the comprehensive study of every detailed aspect prohibitively tedious and costly. As an initial step in the nonlinear analysis of this electrohydrodynamic problem, we have computed various solutions that are considered to be representative of most realistic circumstances. The objective of this work is to provide an overview of the general nonlinear behaviour of leaky dielectric drops, which may be useful to guide more systematic experimentation and further detailed theoretical studies. Since Ajayi's attempt (1978) to extend Taylor's linear asymptotic model to include higher-order terms failed to fully resolve the quantitative discrepancy between the theory and experiment, it has been assumed that nonlinear solutions cannot provide important insights into basic electrohydrodynamic behaviour of drops. Nevertheless, the results of finite-element computations presented in this work clearly demonstrate that significant progress in understanding the electrohydrodynamic behaviour of leaky dielectric drops can be made with systematic nonlinear analysis.

The authors are grateful to the referees for their valuable and constructive comments. This research was supported by the Division of Engineering and Geosciences, Office of Basic Energy Sciences, US Department of Energy, under contract DE-AC05-84OR21400 with Martin Marietta Energy Systems, Inc.

REFERENCES

ABBOTT, J. P. 1978 An efficient algorithm for the determination of certain bifurcation points. *J. Comput. Appl. Maths* **4**, 19–27.

ADORNATO, P. M. & BROWN, R. A. 1983 Shape and stability of electrostatically levitated drops. *Proc. R. Soc. Lond.* A **389**, 101–117.

AJAYI, O. O. 1978 A note on Taylor's electrohydrodynamic theory. *Proc. R. Soc. Lond.* A **364**, 499–507.

ALLEN, R. S. & MASON, S. G. 1962 Particle behaviour in shear and electric fields. I. Deformation and burst of fluid drops. *Proc. R. Soc. Lond.* A **267**, 45–61.

BAILES, P. J. 1981 Solvent extraction in an electric field. *Indust. Engng Chem. Process Des. Dev.* **20**, 564–570.

BAIRD, M. H. I. 1983 Electrostatic effects on extraction. In *Handbook of Solvent Extraction* (ed. T. C. Lo, M. H. I. Baird, & C. Hanson), vol. 20, chap. 8, pp. 268–269. John Wiley & Sons.

BASARAN, O. A. 1984 Electrohydrodynamics of drops and bubbles. PhD thesis, University of Minnesota.

BASARAN, O. A. & SCRIVEN, L. E. 1989 Axisymmetric shape and stability of charged drops in an electric field. *Phys. Fluids* A **1**, 799–809.

BAYGENTS, J. C. & SAVILLE, D. A. 1989 The circulation produced in a drop by an electric field: A high field strength electrokinetic model. In *Drops and Bubbles: Third Intl. Colloq.* (ed. T. G. Wang), pp. 7–17. American Institute of Physics.

BOUDOUVIS, A. G. 1987 Mechanisms of surface instabilities and pattern formation in ferromagnetic liquids. PhD thesis, University of Minnesota. Available from University Microfilms International, Ann Arbor, MI 48106.

BOUDOUVIS, A. G., PUCHALLA, J. L. & SCRIVEN, L. E. 1987 Magnetohydrostatic equilibria of ferrofluid drops in external magnetic fields. *Chem. Engng Commun.* **67**, 129–144.

BUCHNER, E. H. & VAN ROYEN, A. H. H. 1929 Bewegung von Flüssigkeitsstrahlen und Tropfen in einem elektrischen Felde. *Kolloid-Z.* **49**, 249–253.

BUNGENBERG DE JONG, H. G. & HOSKAM, E. G. 1941 Motory phenomena in coacervate drops in a diffusion field and in the electric field. *Konikl. Ned. Akad. Wetenschap. Proc.* **44**, 1099–1103.

CHANG, L. S. & BERG, J. C. 1983 Fluid flow and transfer behaviour of a drop translating in an electric field at intermediate Reynolds numbers. *Intl J. Heat Mass Transfer* **26**, 823–832.

CHANG, L. S. & BERG, J. C. 1985 The effect of interfacial tension gradients on the flow structure of single drops or bubbles translating in an electric field. *AIChE J.* **31**, 551–557.

CHANG, L. S., CARLESON, T. E. & BERG, J. C. 1982 Heat and mass transfer to a translating drop in an electric field. *Intl J. Heat Mass Transfer* **25**, 1023–1030.

CHRISTODOULOU, K. N. 1990 Computational physics of slide coating flow. PhD thesis, University of Minnesota. Available from University Microfilms International, Ann Arbor, MI 48106.

CHRISTODOULOU, K. N. & SCRIVEN, L. E. 1989 The fluid mechanics of slide coating. *J. Fluid Mech.* **208**, 321–354.

CHRISTODOULOU, K. N. & SCRIVEN, L. E. 1992 Discretization of free surface flows and other moving boundary problems. *J. Comput. Phys.* **99**, 39–55.

FENG, J. Q. 1991 A theoretical investigation of raindrop oscillations. PhD thesis, University of Illinois at Urbana-Champaign. Available from University Microfilms International, Ann Arbor, MI 48106.

FENG, J. Q. & BEARD, K. V. 1991 Resonances of a conducting drop in an alternating electric field. *J. Fluid Mech.* **222**, 417–435.

FENG, J. Q. & SCRIVEN, L. E. 1992 Electrostatic effects in continuous liquid coating. *Intl Symp. on Coating Science and Technology. Paper 38d, New Orleans, Louisiana.*

FENG, J. Q. & SCRIVEN, L. E. 1993 Electrostatic effects on coating flow sensitivity to ongoing disturbances. *AIChE Annual Meeting. Paper 42h, St. Louis, Missouri.*

GARTON, C. G. & KRASUCKI, Z. 1964 Bubbles in insulating liquids: stability in an electric field. *Proc. R. Soc. Lond.* A **280**, 211–226.

GRIFFITHS, S. K. & MORRISON, F. A., JR. 1979 Low Peclet number heat and mass transfer from a drop in an electric field. *Trans. ASME* C: *J. Heat Transfer* **101**, 484–488.

HARKER, J. H. & AHMADZADEH, J. 1974 The effect of electric fields on mass transfer from falling drops. *Intl J. Heat Mass Transfer* **17**, 1219–1225.

HE, W., BAIRD, M. H. I. & CHANG, J. S. 1993 The effect of electric field on mass transfer from drops dispersed in a viscous liquid. *Can. J. Chem. Eng* **71**, 366–376.

HOOD, P. 1976 Frontal solution program for unsymmetric matrices. *Intl J. Numer. Methods Engng* **10**, 379–399 (and Correction, *Intl J. Numer. Methods Eng.* **11** (1977), 1055).

HUYAKORN, P. S., TAYLOR, C., LEE, R. L. & GRESHO, P. M. 1978 A comparison of various mixed interpolation finite elements in the velocity-pressure formulation of Navier–Stokes equations. *Comput. Fluids* **6**, 25–35.

IOOSS, G. & JOSEPH, D. D. 1990 *Elementary Stability and Bifurcation Theory* (2nd edn). Springer.

KELLER, H. B. 1977 Numerical solution of bifurcation and nonlinear eigenvalue problems. In *Applications of Bifurcation Theory* (ed. P. Rabinowitz), pp. 359–384. Academic.

KISTLER, S. F. & SCRIVEN, L. E. 1983 Coating flows. In *Computational Analysis of Polymer Processing* (ed. J. R. A. Pearson & S. M. Richardson), pp. 243–299. Applied Science Publishers.

MELCHER, J. R. 1981 *Continuum Electromechanics.* MIT Press.

MELCHER, J. R. & TAYLOR, G. I. 1969 Electrohydrodynamics: a review of the role of interfacial shear stresses. *Ann. Rev. Fluid Mech.* **1**, 111–146.

MIKSIS, M. J. 1981 Shape of a drop in an electric field. *Phys. Fluids* **24**, 1967–1972.

MORRISON, F. A., JR. 1977 Transient heat and mass transfer to a drop in an electric field. *Trans. ASME* C: *J. Heat Transfer* **99**, 269–273.

O'KONSKI, C. T. & HARRIS, F. E. 1957 Electric free energy and the deformation of droplets in electrically conducting systems. *J. Phys. Chem.* **61**, 1172–1174.

O'KONSKI, C. T. & THACHER, H. C. 1953 The distortion of aerosol droplets by an electric field. *J. Phys. Chem.* **57**, 955–958.

ORTEGA, J. M. & RHEINBOLDT, W. C. 1970 *Iterative Solution of Nonlinear Equations in Several Variables.* Academic.

POZRIKIDIS, C. 1992 *Boundary Integral and Singularity Methods for Linearized Viscous flow.* Cambridge University Press.

PTASINSKI, K. J. & KERKHOF, P. J. A. M. 1992 Electric field driven separations: Phenomena and applications. *Sep. Sci. Technol.* **27**, 995–1021.

RIKS, E. 1972 Application of Newton's method to the problem of elastic stability. *J. Appl. Mech.* **39**, 1060–1065.

ROSENKILDE, C. E. 1969 A dielectric fluid drop in an electric field. *Proc. R. Soc. Lond.* A **312**, 473–494.

SANTOS, J. M. DE 1991 Two-phase cocurrent downflow through constricted passages. PhD thesis, University of Minnesota. Available from University Microfilms International, Ann Arbor, MI 48106.

SCOTT, T. C. 1989 Use of electric fields in solvent extraction: A review and prospects. *Sep. Purif. Methods* **18**, 65–109.

SHERWOOD, J. D. 1988 Breakup of fluid droplets in electric and magnetic fields. *J. Fluid Mech.* **188**, 133–146.

STRANG, G. & FIX, G. J. 1973 *An Analysis of the Finite Element Method.* Prentice-Hall.

TAYLOR, G. I. 1964 Disintegration of water drops in an electric field. *Proc. R. Soc. Lond.* A **280**, 383–397.

TAYLOR, G. I. 1966 Studies in electrohydrodynamics. I. The circulation produced in a drop by an electric field. *Proc. R. Soc. Lond.* A **291**, 159–166.

THOMPSON, J. F., WARSI, Z. U. A. & MASTIN, W. C. 1985 *Numerical Grid Generation.* Elsevier.

THORNTON, J. D. 1968 The application of electrical energy to chemical and physical rate processes. *Rev. Pure Appl. Chem.* **18**, 197–218.

TORZA, S., COX, R. G. & MASON, S. G. 1971 Electrohydrodynamic deformation and burst of liquid drops. *Phil. Trans. R. Soc. Lond.* A **269**, 295–319.

TSUKADA, T., KATAYAMA, T., ITO, Y. & HOZAWA, M. 1993 Theoretical and experimental studies of circulations inside and outside a deformed drop under a uniform electric field. *J. Chem. Engng Japan* **26**, 698–703.

TSUKADA, T., YAMAMOTO, Y., KATAYAMA, T. & HOZAWA, M. 1994 Effect of an electric field on the behaviour of a drop moving in a quiescent liquid. *J. Chem. Engng Japan* **27**, 662–666.

UNGAR, L. H. & BROWN, R. A. 1982 The dependence of the shape and stability of captive rotating drops on multiple parameters. *Phil. Trans. R. Soc. Lond.* A **306**, 347–370.

VIZIKA, O. & SAVILLE, D. A. 1992 The electrohydrodynamic deformation of drops suspended in liquids in steady and oscillatory electric fields. *J. Fluid Mech.* **239**, 1–21.

WALTERS, R. A. 1980 The frontal method in hydrodynamics simulations. *Comput. Fluids* **8**, 265–272.

WEATHERLEY, L. R. 1992 Electrically enhanced extraction. *Science and Practice of Liquid-Liquid Extraction,* vol. **2** (ed. J. D. Thornton), chap. 5, §5.6, pp. 407–419. Oxford University Press.